Cathepsin L is required for endothelial progenitor cell-induced neovascularization

Carmen Urbich, Christopher Heeschen, Alexandra Aicher, Ken-ichiro Sasaki, Thomas Bruhl, Wolf K. Hofmann[§], Christoph Peters[#], Thomas Reinheckel[#], Len A. Pennacchio[*], Nasreddin D. Abolmaali[&], Emmanouil Chavakis, Andreas M. Zeiher, and Stefanie Dimmeler

Molecular Cardiology, Department of Internal Medicine IV, University of Frankfurt, Theodor-Stern-Kai 7, Frankfurt, Germany,
[§]Department of Hematology and Oncology, Internal Medicine III, University of Frankfurt, Theodor-Stern-Kai 7, Frankfurt, Germany,
[#]Department of Molecular Medicine and Cell Research, Albert-Ludwigs-University Freiburg, Stefan Meier Strasse 17, Germany,
[*]Department of Genome Sciences, Lawrence Berkeley National Laboratory, Berkeley, USA
[&]Institute for Diagnostic and Interventional Radiology, University of Frankfurt, Theodor-Stern-Kai 7, Frankfurt, Germany.

Words: main text: 3647

Address for correspondence:

Stefanie Dimmeler, PhD
Molecular Cardiology
Dept. of Internal Medicine IV
University of Frankfurt
Theodor Stern-Kai 7
60590 Frankfurt
Germany
Fax: +49-69-6301-7113 or -6374
Phone: +49-69-6301-7440 or -5789
E-mail: Dimmeler@em.uni-frankfurt.de

C.U.: urbich@em.uni-frankfurt.de
C.H.: c.heeschen@em.uni-frankfurt.de
A.A.: aicher_a@yahoo.com
K.S.: Sasakende@aol.com
T.B.: Tom.Bruehl@gmx.de
W.K.H.: W.K.Hofmann@em.uni-frankfurt.de
C.P.: christoph.peters@mol-med.uni-freiburg.de
T.R.: reinheck@ukl.uni-freiburg.de
L.A.P.: LAPennacchio@lbl.gov
N.D.A.: abolmaali@em.uni-frankfurt.de
E.C. chavakis@em.uni-frankfurt.de
A.M.Z.: zeiher@em.uni-frankfurt.de
S.D.: dimmeler@em.uni-frankfurt.de

Abstract (149 words)

Infusion of endothelial progenitor cells (EPCs), but not of mature endothelial cells (ECs), promotes neovascularization after ischemia. We performed a gene expression profiling of EPCs and ECs to identify genes, which might be important for the neovascularization capacity of EPCs. Intriguingly, the protease cathepsin L (CathL) was highly expressed in EPCs as opposed to ECs and is essential for matrix degradation and invasion by EPCs in vitro. CathL-deficient mice showed impaired functional recovery after hind limb ischemia supporting the concept for an important role of CathL in postnatal neovascularization. Infused CathL-deficient progenitor cells failed to home to sites of ischemia and to augment neovascularization. In contrast, overexpression of CathL in mature ECs significantly enhanced their invasive activity and induced their neovascularization capacity in vivo. Taken together, CathL plays a crucial role for the integration of circulating EPCs into the ischemic tissue and is required for neovascularization mediated by EPCs.

Introduction

Postnatal neovascularization is an important process to rescue tissue from critical ischemia [1]. Adult blood vessel formation was thought to be mainly attributed to the migration and proliferation of preexisting, fully differentiated endothelial cells, a process referred to as angiogenesis [2-4]. However, recent studies provide increasing evidence that circulating bone marrow-derived endothelial progenitor cells (EPCs) significantly contribute to adult blood vessel formation [5,6]. Transplantation of EPCs after ischemia improves neovascularization and cardiac function in animal models [7,8]. Initial clinical studies suggest that EPCs also improve vascularization after myocardial infarction in humans [9]. These endothelial progenitor cells can be grown from hematopoietic stem cells or peripheral blood mononuclear cells (PBMCs) [5,6]. Cultivated EPCs derived from peripheral blood were shown to express various endothelial marker proteins such as VEGF receptor 2 (KDR), von Willebrand factor (vWF), VE-cadherin, and endothelial nitric oxide synthase (Nos3), similar to mature endothelial cells (EC) [7,10,11]. However, only EPCs, but not mature ECs improve neovascularization in vivo, although they both share a comparable expression of endothelial marker proteins and a similar in vitro angiogenic capacity [7]. Therefore, in order to gain insights into the molecular differences between EPCs and mature ECs, we performed a gene expression analysis. Our data indicate that one potential reason for the in vivo difference between EPCs and mature ECs could be the expression of lysosomal cysteine or aspartyl-proteases of the cathepsin family.

The lysosomal proteases comprise the catalytic classes of serine, aspartic as well as cysteine peptidases exhibiting endo- or exopeptidase activities or a combination of both. Yet, there is growing evidence for specific intra- and extracellular functions for these lysosomal enzymes, especially leading to tumor invasion and metastasis [12-14]. In detail, cathepsin D (CathD) promotes tumor progression by modulating proliferation and angiogenesis [15] and cathepsin L (CathL) anti-sense oligonucleotides inhibit invasion of osteosarcoma cells [16]. For their extracellular actions, lysosomal peptidases are secreted in considerable amounts. Early investigations on the cysteine peptidase CathL revealed that this protease is identical to the “major excreted protein” of malignantly transformed mouse fibroblasts [17]. Neovascularization involves the activation, proliferation, and migration of ECs as well as homing and transmigration of circulating EPCs in concert with localized proteolytic modification of the extracellular matrix (ECM). Proteolysis of ECM facilitates endothelial cell migration and proliferation, releasing stored angiogenic and anti-angiogenic signaling molecules from latent

reserves as well as loosening the stromal milieu to facilitate migration [18]. Moreover, CathL exerts specific physiological functions, including the regulation of epidermal homeostasis, hair follicle cycling, cardiac function, and MHC class II-mediated antigen presentation [19-23].

The present study now demonstrates that CathL is required for invasion of EPCs into ischemic tissues, because pharmacological inhibition or genetic ablation of CathL prevented EPC-enhanced neovascularization of ischemic areas.

Results

Gene expression analysis of EPCs versus HUVECs

Human EPCs were cultivated from peripheral blood mononuclear cells as previously described [10,11]. Phenotypical characterization confirmed the expression of various endothelial marker proteins including VEGF receptor 2 (KDR), CD105, VE-cadherin, vWF, CD146, CD31, and Nos3 (Fig. 1*a*; data not shown; [9-11]). Transplantation of these EPCs into immunodeficient nude mice significantly improved neovascularization in a hind limb ischemia model (Fig. 1*b*). In contrast, infusion of human umbilical venous endothelial cells (HUVEC) did not improve neovascularization (Fig. 1*b*). In order to explore the expression differences between EPCs and HUVECs at mRNA level, we performed a global gene expression analysis of about 10,000 genes. We additionally compared the gene expression profile of $CD14^+$ monocytic cells, since monocytes may contaminate the EPC culture (<5 %). We identified 480 highly differentially expressed genes (5-fold up) in EPCs compared to HUVECs. A gene tree analysis revealed that EPCs selectively express higher levels of the lysosomal peptidases, including several cathepsins (Fig. 1*c/d*).

Especially, the lysosomal aspartic protease cathepsin D as well as the lysosomal cysteine proteases cathepsin H, cathepsin L, and cathepsin O were significantly upregulated in EPCs (Fig. 1*c*). In contrast, cathepsin B, E and G were not significantly different in EPCs compared to HUVECs. CathD and CathL are important for tumor invasion and metastasis [15,16]. Therefore, we selectively confirmed the expression of these cathepsins on protein level. EPCs showed significantly increased protein levels of cathepsin D and cathepsin L compared to HUVEC, human microvascular endothelial cells (HMVEC) and isolated $CD14^+$ monocytes as assessed by Western blot (Fig. 2*a-d*) and immunoassay (Fig. 2*e/f*).

The activity of lysosomal cysteine proteases is post-transcriptionally controlled by cystatins, which act as general inhibitors of various cathepsin members. However, the expression of cystatin 1, cystatin 6, and cystatin D are lower or equally expressed in EPCs versus HUVEC (Fig. 1*d*). Only cystatin B, C, and F showed a 2.4-, 2.8- and 3.7-fold increased expression in EPCs, respectively (Fig. 1*d*).

Overall, cathepsin L (CathL)-activity was significantly higher (>10-fold) in EPCs as compared to HUVEC (Fig. 2*g*). Consistently, the p41 splice variant (p41(65aa)) of major histocompatibility complex class II-associated invariant chain (Ii), which is known to bind to CathL and permits the maintenance of a pool of mature activated CathL under neutral pH [24], was increased in EPCs (Fig. 2*h*). In contrast, despite increased protein expression, the

activity of cathepsin D was only slightly elevated in EPCs as compared to HUVEC (EPC: 1.86-fold compared to HUVEC), therefore, we further focused on CathL.

Role of CathL for vasculogenesis and angiogenesis

Next, we investigated the role of CathL for neovascularization in a hind limb ischemia model. Gene ablation revealed a significant impairment of neovascularization in $CathL^{-/-}$ mice (Fig. 3*a*), demonstrating that CathL is essential for ischemia-induced neovascularization.

Vasculogenesis, an important feature of ischemia-induced neovascularization [5], depends on various critical steps (Fig. 3*b*). Because cathepsins exert a widespread substrate specificity, and, thereby, may influence different cellular processes, we determined the potential involvement of CathL in each individual step. First, we assessed the mobilization of stem cells from the bone marrow in wt and $CathL^{-/-}$ mice. However, mobilization induced by hematopoietic growth factors (SCF: 300 µg/kg and G-CSF: 250 µg/kg daily for 3 days) was not impaired in $CathL^{-/-}$ mice (wt: 258.8±37% $CathL^{-/-}$: 342.6±65% increase in c-$kit^+Sca\text{-}1^+$ (stem cell antigen-1^+) cells in peripheral blood). Moreover, adhesion of cultivated EPCs to different matrices or TNFα-stimulated HUVECs was not modulated by pretreatment with the CathL-inhibitor (Fig. 3*c*, data not shown). Next, we tested whether the adhesion of EPCs to denuded arteries in vivo is modulated by CathL inhibition. For that purpose, EPCs were pretreated with the cell-permeable irreversible CathL-inhibitor Z-Phe-Phe-CH_2F (Z-FF-FMK) for 2 hours, washed twice, and were infused intravenously in nude rats 24 hours after vessel denudation. However, CathL-inhibitor pretreatment did not affect the homing and adhesion of EPCs to the denuded arteries in vivo (Fig. 3*d/e*), although control experiments confirmed that the inhibition of CathL is irreversible and lasts for more than 20 hours (data not shown). These data indicate that CathL is not required for the adhesion of EPC in vitro and in vivo.

Next, we determined the role of CathL for proliferation, apoptosis and migration of human EPCs and murine bone marrow-derived hematopoietic progenitors. Control experiments confirmed the expression of CathL in murine $Sca\text{-}1^+$, $Sca\text{-}1^+Lin^-$ and $Sca\text{-}1^+flk\text{-}1^+$ cells (Supplementary Fig. 1). However, pharmacological inhibition of CathL in human EPCs or genetic ablation using $CathL^{-/-}$ cells did not lead to a significant change in any of these parameters (Fig. 3*f*). To further address, whether CathL activity can enhance the release of growth promoting factors from EPCs, which then could act in a paracrine manner on mature ECs, we determined the pro-angiogenic activity of conditioned medium derived from EPCs, which were cultivated in the presence or absence of the CathL-inhibitor Z-FF-FMK. The supernatant (10x concentrated) of untreated EPCs contained high concentrations of VEGF

and SDF-1, respectively, and increased migration of mature ECs and tube formation in an in vitro angiogenesis assay (data not shown). However, conditioned medium derived from EPCs, that were treated for 2 hours with Z-FF-FMK, did not reduce the ability of the medium to promote angiogenesis (data not shown). Thus, our data rule out that CathL is critically involved in the regulation of EPC survival, proliferation, migration and the release of angiogenic growth factors.

Since cathepsins are matrix degrading enzymes, we investigated whether CathL contributes to the invasive capacity of EPCs in vitro by using a modified Boyden chamber filled with matrigel [25,26]. EPCs demonstrated a more than 20-fold higher invasive capacity as compared to HUVECs and a significantly higher invasion than $CD14^+$ monocytes (Fig. 4*a*). Incubation of EPCs with the CathL-inhibitor significantly reduced the invasive capacity of EPCs (Fig. 4*a*). In addition, incubation of EPCs with cystatin C, which is a general inhibitor of papain-like cysteine peptidases (e.g. cathepsin B, H, L), also significantly decreased EPC invasion, whereas the cathepsin S (CathS)-inhibitor Z-Phe-Leu-COCHO [27], MMP-inhibitors (GM6001, GM1489, MMP-3 inhibitor, MMP-9 inhibitor) or elastase inhibitors did not significantly affect EPC invasion (Fig. 4*a* and data not shown). A toxic effect of the inhibitors on EPC survival was excluded by measuring apoptosis and necrosis (data not shown). Consistently, the invasion of $CathL^{-/-}Sca\text{-}1^+$ cells was significantly reduced as compared to wt cells (Fig. 4*b*). These data suggest that CathL contributes to the invasive capacity of EPCs.
In order to identify the CathL targets involved in mediating EPC invasion, we determined the matrix degradation activity and a possible interference of cathepsins with other proteases. Extracts of EPCs induced the degradation of the matrix components gelatin and collagen, which are targets of CathL [28], as assessed by zymography (Fig. 4*c*). The proteolytic activity was abolished by the CathL-inhibitor (Fig. 4*c/d*), clearly demonstrating that the matrix degrading activity in EPCs toward these substrates is completely dependent on CathL. Similar results were obtained, when EPC cell culture supernatants were used (data not shown), demonstrating that CathL can act extracellularly. In contrast, CathL inhibition did not affect MMP-2 and MMP-9 activity in EPCs (Fig. 4*e*). Taken together, these data suggest that CathL specifically contributes to the invasive activity of EPCs by degrading matrix proteins such as gelatin or collagen.

To investigate whether the impaired neovascularization in CathL-deficient mice is also related to a reduction in angiogenesis, namely the proliferation, migration and sprouting of mature ECs, we determined the in vitro angiogenic activity of mature ECs. However, incubation of HUVEC with the CathL-inhibitor (Z-FF-FMK) or cystatin C did not affect proliferation or

migration (Supplementary Fig. 2*a/b*). In addition, the incubation of HUVEC with Z-FF-FMK or the cysteine protease inhibitor L-trans-epoxysuccinyl-leucyl amido(4-guanidio)butane (E64) did not reduce tube formation in an in vitro sprouting assay, whereas the broad-spectrum MMP-inhibitor chlorhexidine (CHX) did reduce tube formation (Supplementary Fig. 2*c/d*). In addition, the CathL-inhibitor Z-FF-FMK, cystatin or E64 did not inhibit tube formation as assessed with a human in vitro angiogenesis assay (data not shown). Likewise, mature aortic EC isolated from CathL$^{-/-}$ mice showed no functional impairment with respect to migration, proliferation or invasion and no increase in apoptosis (Supplementary Fig. 2*e-h*). Moreover, the degradation products of extracellular matrix proteins, which had been incubated with purified CathL enzyme, did not significantly increase in vitro angiogenesis (113.1±4.1% of matrix without enzyme; n=3). Likewise, tube formation of ECs cultivated on matrix proteins was not altered in the presence of the purified CathL enzyme (88.1±13.2% of control; n=3). These data suggest that CathL is not involved in regulation of the angiogenic response of mature ECs rather than specifically affecting EPC-mediated vasculogenesis.

CathL is essential for EPC-mediated neovascularization in vivo

Having demonstrated that CathL specifically affects EPC invasion, we investigated the effect of CathL on integration and function of EPCs during neovascularization in vivo. EPCs were incubated ex vivo with Z-FF-FMK (10 µM) or vehicle for 2 h prior to infusion. Twenty-four hours after unilateral induction of hind limb ischemia in nude mice, EPCs were intravenously injected. Mice receiving EPCs pretreated with the CathL-inhibitor showed significantly less improvement in limb perfusion as compared to mice receiving vehicle-treated EPCs (Fig. 5*a/b*). Consistently, capillary density increased to a greater extent in mice receiving untreated EPCs as compared to CathL-inhibitor-treated EPCs (Fig. *5c* and supplementary Fig. 3). In addition, the number of small conductance vessels (< 50 µm) was significantly increased in mice receiving untreated EPCs, whereas CathL-inhibitor-pretreatment of EPCs prevented this increase (Supplementary Fig. 4). Early EPC homing to the site of ischemia was investigated in vivo by magnetic resonance imaging (MRI). Twenty-four hours after induction of ischemia, EPCs labeled with magnetic beads and pretreated with DMSO or the CathL-inhibitor Z-FF-FMK were intravenously injected. MRI scans were performed after another 24 hours. In the "Turbo Inversion Recovery Magnitude" (TIRM) images, the area of ischemia is visualized by a strong hyperintensity compared to the contralateral limb (Fig. 5*d*; upper panel). In the T2* weighted images, the homing of untreated EPCs led to a marked signal extinction, whereas in animals receiving EPCs pretreated with the CathL-inhibitor Z-FF-FMK no signal loss was observed suggesting a significant reduction in early EPC homing (Fig. 5*d*; lower panel).

Immunohistochemistry of muscle sections after 14 days further revealed that the incorporation of human EPCs into vascular structures was significantly reduced in mice receiving EPCs pretreated with the CathL-inhibitor as assessed by double-staining against human HLA or labeling with CM-DiI to detect the transplanted human EPCs, and CD146, vWF or CD31 (Fig. 5*e/f* and supplementary figure 5). Control experiments confirmed that the viability of the inhibitor-treated cells was not affected (control: 1.1±0.4% vs. 1.2±0.4% annexin^{+}/7AAD^{+} cells of inhibitor-treated EPCs) and that CathL-activity was completely inhibited after 2 hours of Z-FF-FMK incubation (94.1±2.9% inhibition, $p<0.05$, $n=4$).

In a gene-based approach, we assessed the functional activity of bone marrow mononuclear cells derived from male wild-type mice or from male CathL$^{-/-}$ mice. Consistent with the data for the pharmacological inhibition of CathL, the improvement of neovascularization of the ischemic hind limb after 2 weeks was significantly reduced in mice treated with CathL$^{-/-}$ cells as compared to mice treated with cells from wild-type controls (Fig. 5*g*). Accordingly, the capillary density was significantly lower in animals treated with bone marrow cells from CathL$^{-/-}$ mice (mice treated with wild-type cells: 261±46%; mice treated with CathL$^{-/-}$ cells: 133±16%; $P=0.032$). Finally, we determined the number of Y-chromosome-positive transplanted cells derived from male CathL-deficient mice, which were incorporated in the host microvessels, by fluorescence-in-situ-hybridization (FISH) (Supplementary figure 6). The incorporation of CathL$^{-/-}$ cells was significantly reduced to 52.7±13.2% in comparison to wild-type cells.

In order to determine the specific involvement of MMP-9, which is known to be important for angiogenesis [29], or CathD for progenitor cell-mediated augmentation of neovascularization, we isolated cells from MMP-9- or CathD-deficient mice and infused these cells into nude mice after induction of hind limb ischemia. However, neither CathD$^{-/-}$ nor MMP-9$^{-/-}$ bone marrow-derived cells showed a reduction in their neovascularization capacity as compared to wild-type cells (Fig. 5*g*).

Finally, we determined the contribution of bone marrow-derived circulating progenitor cells for increased protease activity in ischemic tissues in vivo. Therefore, mice were lethally irradiated to ablate the bone marrow before induction of hind limb ischemia. Control experiments confirmed the complete reduction of colony forming activity within the bone marrow after irradiation (data not shown). 48 hours after induction of ischemia, muscle lysates of the ischemic and non-ischemic limbs were prepared and subjected to zymographies and Western blot analysis. As shown in the supplementary figure 7, CathL as well as MMP-9 activity were significantly induced in the ischemic tissue. In irradiated mice, MMP-9 activity was still significantly up-regulated after ischemia (supplementary Fig. 7), indicating that MMP-9 is

increased independent of bone marrow-derived cells, but probably derives from tissue-residing cells. In contrast, the ischemia-induced augmentation of CathL activity was abolished in irradiated mice (supplementary Fig. 7). These data demonstrate that the increase of CathL in ischemic tissue is mediated by irradiation-sensitive, likely bone marrow-derived cells.

Overexpression of CathL in mature endothelial cells partially rescued the impaired improvement of neovascularization

In order to investigate whether overexpression of CathL might rescue the failure of mature ECs to promote neovascularization after intravenous infusion, HUVEC were transiently transfected with CathL before injection in a hind limb ischemia model. The infusion of CathL-transfected HUVECs significantly increased the recovery of limb perfusion as compared to vector-transfected cells (Fig. 6*a*). Control experiments confirmed that the transfection of CathL in HUVECs resulted in an increased CathL expression and activity (Fig. 6*b/c*) and subsequently enhanced their invasive capacity in vitro (Fig. 6*d*). Likewise, infusion of isolated mature aortic ECs from CathL overexpressing transgenic mice improved neovascularization (135±16% of control, n=3).

Discussion

Proteases are of major importance for the formation of new blood vessels [30-32]. In order to form sprouts, endothelial cells must penetrate the extracellular matrix consisting of type IV collagen, laminin, fibronectin and many other macromolecules. To achieve this goal, mature endothelial cells are equipped with a set of proteases including matrix metalloproteinases (MMPs) and the urokinase-type plasminogen activator (uPA). The data of the present study now indicate that circulating progenitor cells express a different pattern of proteases. Ex vivo cultivated circulating EPCs showed profoundly increased levels of cathepsins as compared to mature ECs. These broad-spectrum proteases are potent in degrading several extracellular matrix proteins (laminin, fibronectin, collagens I and IV, elastin and other structural proteins of basement membranes (reviewed in [13,33]). Indeed, the matrix degrading activity of EPCs towards gelatin or collagen was abolished by inhibition of CathL. The activity of cathepsins is determined by the balance with endogenous inhibitors. Whereas CathL expression was 9-fold higher in EPCs compared to HUVECs, the endogenous protein-based cathepsin inhibitors (cystatins) showed either no different expression or only a minor increase in expression up to 2 to 3-fold (Fig. 1*d*). Consistently, CathL activity was significantly higher in EPCs. In contrast, CathD activity was slightly elevated despite a significantly increased expression. Thus, whereas CathL activity is maintained in EPCs, CathD appears to be inactivated by a post-transcriptional mechanism. One may speculate that CathL is protected against destabilization at neutral pH in the extracellular milieu by binding to p41, a splice variant of major histocompatibility complex class II-associated invariant chain [24], which is expressed in EPCs (Fig. 2*h*).

Given the overlapping substrate specificity of lysosomal proteases, it is surprising that CathL appears to be of particular importance. However, previous studies using CathL knockout animals provide evidence for biological effects being specifically mediated by CathL [22,23]. In line with these findings, our results demonstrate that the improvement of neovascularization is significantly reduced in homozygous CathL knockout mice. Moreover, pharmacological inhibition of CathL abolished the matrix degrading activity of EPC extracts or cell culture supernatants. CathS was recently shown to contribute to angiogenesis [34]. However, pharmacological inhibition of CathS did not affect EPC invasion. Moreover, genetic ablation of another related member of the cathepsin family, CathD, did not reduce the functional activity of bone marrow-derived stem cells to promote neovascularization after ischemia. These data suggest that CathL exhibits a specific function in EPCs. Our data further indicate that pharmacological inhibition of other proteases such as elastases or MMPs did not affect the

invasive activity of EPCs in vitro. In line with these in vitro findings, MMP-9-deficient progenitor cells showed no impairment to augment neovascularization in vivo. Likewise, the increase of MMP-9 activity after induction of ischemia was independent of bone marrow-derived cells, but rather reflects an increased release by tissue-residing cells. This is in contrast to the up-regulation of CathL after ischemia, which was abolished by irradiation-induced bone marrow ablation. Although we cannot formally rule out the involvement of other proteases for neovascularization, since the pharmacological inhibition or genetic ablation of CathL did not completely abrogate the improvement of neovascularization induced by EPCs, our data indicate that CathL plays a specific role opposed to other cathepsins or MMP-9.

The impairment of neovascularization in CathL$^{-/-}$ mice may be related to 1) a reduction in functional activity of mature endothelial cells from CathL$^{-/-}$ mice resulting in impaired angiogenesis or 2) a reduced capacity of EPC to promote vasculogenesis. Since we demonstrated that pharmacological CathL-inhibitors and genetic depletion of CathL did not affect the pro-angiogenic activity of mature endothelial cells, an interference of CathL with the classical angiogenesis appears unlikely. In contrast, CathL appears to specifically contribute to vasculogenesis by promoting the invasive activity of EPCs, whereas EPC mobilization, adhesion, transmigration, survival and migration were not affected. Inhibition or genetic ablation of CathL, thus, specifically reduced the invasive potential of EPCs in vitro and reduced the functional improvement of neovascularization by infused EPCs in vivo. The finding that the number of incorporated CathL$^{-/-}$ cells is reduced compared to wild-type cells suggests that CathL expression is required for penetration and tissue invasion of EPCs. The degradation of extracellular matrix by cathepsins can also lead to the release of angiogenesis-modulating molecules such as endostatin by CathL and angiostatin by CathD [35,36]. However, we did not observe a significant CathL-dependent change in angiogenic activity of conditioned medium from EPCs or after degradation of matrix proteins in vitro. Specifically, a 1.27-fold, non-significant elevation of pro-angiogenic activity was noted, when conditioned medium from EPCs was used, which had been incubated with a CathL-inhibitor. These results are in line with a previous study showing the release of an anti-angiogenic factor by CathL-induced degradation of collagen [36]. Thus, the essential role of CathL for neovascularization is not due to a dysregulation of angiogenesis or release of pro-angiogenic paracrine factors. Our data indicate that CathL is responsible for functional integration of EPCs into newly formed capillaries. Blockade of tissue invasion of EPCs in turn may reduce neovascularization capacity and neovascularization in CathL$^{-/-}$ mice. Indeed, a recent study demonstrated that genetic ablation of progenitor cell mobilization can abrogate tissue neovascularization [37].

Taken together, the present study for the first time demonstrates a critical role of CathL for the invasive and functional capacity of EPCs. The high expression levels of CathL exquisitely equippe the cells for “drilling for oxygen” in order to improve blood supply to ischemic tissues. In contrast, inhibition of the invasive potential of circulating progenitor cells by CathL-inhibitors may be an attractive target for limiting tumor vascularization, which is critically dependent on EPC invasion [37,38].

Acknowledgement

We are thankful to Dr. Jens Gille (University of Frankfurt, Frankfurt, Germany) and Dr. Zena Werb (University of California, San Francisco, USA) for providing the MMP9-deficient mice. We would like to thank Andrea Knau, Melanie Näher, and Marion Muhly-Reinholz for excellent technical help. This study was supported by the Deutsche Forschungsgemeinschaft (Di 600/4-1), the Alfried Krupp Stiftung (S.D.), the Fonds der Chemischen Industrie (T.R. and C.P.), by the Deutsche Krebshilfe (T.R.), and in part by NIH Grant HL071954A administered through the U.S. Department of Energy under contract no. DE-AC03-76SF00098 (L.A.P.).

Methods

Generation of CathL-deficient mice and transgenic mice overexpressing the human CathL

CathL-deficient mice have been generated by gene targeting in mouse embryonic stem cells as described [20,21]. Expression of CathL mRNA, protein and activity was completely abolished in CathL-deficient mice [21]. CathL-transgenic mice were generated as previously described [39]. CathD- and MMP-9-deficient mice have been generated as described [40,41].

Cell culture

PBMCs were isolated by density gradient centrifugation from healthy human volunteers [11]. $8x10^6$ PBMCs/ml were plated on human fibronectin (Sigma, Taufkirchen, Germany) and maintained in endothelial basal medium (EBM; CellSystems, St. Katharinen, Germany) with EGM SingleQuots and 20% FCS. After 3 days, nonadherent cells were removed and adherent cells were incubated in fresh medium for 24 h before starting experiments. EPCs were characterized by dual-staining for 1,1'–dioctadecyl–,3,3',3'–tetramethylindocarbocyanine-labeled acetylated low-density lipoprotein (Dil-Ac-LDL) and lectin and expression of endothelial markers KDR, VE-Cadherin, Nos3, and von Willebrand factor [11]. Pooled HUVEC and HMVEC were purchased from CellSystems and cultured as described [42]. $CD14^+$ monocytes were purified from MNCs by positive selection with anti-CD14-microbeads (Miltenyi Biotec, Bergisch-Gladbach, Germany). Sca-1^+ cells were purified from total bone marrow cells by positive selection with anti-sca-1^+-microbeads (Miltenyi Biotec, Bergisch-Gladbach, Germany). Purity assessed by FACS analysis was >95%. Outgrowth of ECs from aortic tissue was performed as previously described [43].

Oligonucleotide microarrays

Ten microgram of total RNA was hybridized to the HG-U95Av2 microarray (Affymetrix, Santa Clara, California; 9670 human genes). The standard protocol used for sample preparation and microarray processing is available from Affymetrix. Expression data were analyzed using Microarray Suite version 5.0 (Affymetrix) and GeneSpring version 4.2 (Silicon Genetics, San Carlos, California) as previously described [44].

Western blot analysis and ELISA

Cells were lyzed as previously described [42]. Blots were incubated with antibodies against CathD, CathL (BD Biosciences, Heidelberg, Germany) or tubulin (Neomarkers, Fremont, California). The autoradiographs were scanned and semiquantitatively analyzed. CathD and

CathL expression was measured with an ELISA according to the manufacturer (Oncogene Research Products, San Diego, California).

CathL-activity

Cell lysates were incubated with the fluorogenic substrate Z-Phe-Arg-4-methoxy-ß-naphthylamide-hydrochloride (50 µM; Sigma) in the presence of 4 M urea at pH 4.7 [45,46]. Fluorescence was measured using a fluorometer with an excitation of 360 nm and an emission at 405 nm.

Proliferation, migration, invasion, apoptosis and tube formation

Proliferation was quantified with a colorimetric cell proliferation ELISA or FACS analysis of BrdU incorporation (Roche Diagnostics, Mannheim, Germany and BD Biosciences, respectively) as previously described [47]. For EC migration, cells were placed in the upper chamber of a modified Boyden chamber as previously described [11]. The formation of tube-like structures was determined with a matrigel assay. HUVEC (10^5 cells/ml) were seeded in medium on *Matrigel Basement Membrane Matrix* (BD Biosciences) in the presence or absence of inhibitors as indicated. Apoptosis was detected by FACS analysis using Annexin-PE binding as described [47].

Plasmid transfection

A plasmid encoding human full length pro-CathL was cloned by PCR from cDNA of EPCs into pcDNA3.1-Myc-His (Invitrogen, The Netherlands). Transient transfection of HUVEC was performed as described previously [47] using Superfect™ (Qiagen, Hilden, Germany).

RT-PCR

The mRNA expression of the p41 splice variant (p41(65aa)) was detected by semi-quantitative RT-PCR (primers: p41-forward 5‘-ACCAAGTGCCAGGAAGAGGTCAGC-3‘ and p41-reverse 5‘-TGACTCACTGCAGTTATGGTGCCCG-3‘).

In vitro invasion

A modified Boyden chamber (Transwell, 8 µm pore size, BD Falcon) was filled with matrigel (4 mg/ml; BD Biosciences). Detached cells (10^5 cells) were placed in the upper compartment of the chamber in the presence or absence of the inhibitors cystatin C, CathL-inhibitor Z-FF-

FMK or Z-FL-COCHO (all Calbiochem, Schwalbach, Germany). After 24 hours at 37°C, chambers were removed and cells at the bottom of the culture plate were stained with Dil-Ac-LDL and counted manually in three random microscopic fields by two independent investigators.

EPC adhesion

EPCs were washed and detached at day 4, labeled with CellTracker green CMFDA (Molecular probes, Portland, Oregon) and plated on fibronectin, collagen or laminin-coated dishes (each 10 µg/ml) for 40 min. Plates were washed and adherent cells were counted manually in three random microscopic fields by two independent investigators.

Zymography

Cell cultured supernatants were concentrated (10x) using Ultrafree-4 centrifugal filter tubes with Biomax-5 membrane (Millipore, Schwalbach, Germany). Cells were lyzed in buffer with urea (4 M urea, 100 mM sodium acetate, 1 mM EDTA, 0.5% Triton X-100). Metalloproteinase activity was analyzed by gelatinolytic zymography as described [48]. The gelatin and collagen zymography for acidic proteases was performed according to Dennhöfer et al. [49]. After gelelectrophoresis, the gels were washed twice for 20 min with 25% isopropanol to remove SDS [50].

Murine model of hind limb ischemia

The murine model of hind limb ischemia was performed by use of 8–10 wk old athymic NMRI nude mice (The Jackson Laboratory, Bar Harbor, Maine). The proximal femoral artery including the superficial and the deep branch as well as the distal saphenous artery were ligated. Cells were intravenously injected 24 hours after induction of hind limb ischemia. Animals received human untreated EPCs and pretreated EPCs (Z-FF-FMK; 10 µM; 2h) or sex-mismatched crude bone marrow cells (10^6 cells/mouse) from male CathL-deficient and wild-type mice, respectively. Bone marrow was harvested aseptically by flushing tibias and femurs of donor mice and filtered (100 µm).

Limb perfusion. After two weeks, ischemic (right)/normal (left) limb blood flow ratio was measured with a laser Doppler blood flow meter (MoorLDI™-Mark 2, Moor Instruments, Inc., Wilmington, Delaware). After twice recording laser Doppler color images, the average perfusions of the ischemic and non-ischemic limb were calculated on the basis of colored histogram pixels.

Denudation model

To study homing and adhesion of infused EPCs, we used a rat model of iliac artery injury. In immunodeficient athymic rnu:rnu rats (5 to 7 weeks old males; 120 to 150 g; Charles River, Sulzfeld, Germany), endoluminal injury to the external iliac artery was produced by three passages of a 0.25-mm-diameter angioplasty guidewire (Advanced Cardiovascular Systems, Santa Clara, California). Briefly, the common and superficial femoral arteries were dissected free along its length and temporarily clamped at the level of the inguinal ligament. Then, an arteriotomy was made distal to the epigastric branch. The angioplasty guidewire was inserted, the clamp removed, and the wire advanced to the level of the aortic bifurcation and pulled back. This was repeated two more times. After removal of the wire, the arteriotomy site was ligated with a 7.0 silk suture (Ethicon). Twenty-four hours after endoluminal injury, a total of $2x10^6$ CM-DiI-labeled (Molecular Probes) human EPCs that were either untreated or pretreated with the CathL-inhibitor Z-FF-FMK (10 µM; 2h) were intravenously infused in each animal. After 7 days, the external iliac arteries were harvested. Cryosections (5 µm) were stained for the endothelial marker von Willebrand factor (Acris Antibodies, Hiddenhausen, Germany) and the number of incorporated EPCs (CM-DiI positive) per section was assessed. A total of three sections per rat were analyzed. SYTOX (Molecular Probes) was used for nuclear staining.

EPC tracking by Magnetic Resonance Imaging (MRI)

EPCs were labeled with 0.9 µm superparamagnetic di-vinyl benzene inert polymer microspheres (Bangs Laboratories, Fishers, Indiana) [51] and intravenously injected 24 hours after induction of limb ischemia. After another 24 hours, mice were placed inside a small loop coil at a 1.5 Tesla system (Magnetom Sonata, Siemens, Erlangen, Germany). 2D-MRI was performed using TIRM-sequences (Turbo Inversion Recovery Magnitude) to visualize the edema related to the ischemia and T2*-weighted gradient echo sequences to visualize the magnetic field distortion related to the superparamagnetic particles-labeled EPCs.

Histological evaluation

Capillary density was determined in 8-µm frozen sections of the adductor and semimembraneous muscles. Endothelial cells were stained for CD146 (Chemicon, Hofheim, Germany) or CD31 (BD Biosciences), respectively. Capillary density is expressed as number of capillaries/myocyte. Human EPCs were identified by co-staining for HLA-A,B,C (APC-labeled; BD Biosciences).

Statistical analysis

Results for continuous variables are expressed as means±SEM or as stated otherwise. Comparisons between groups were analyzed by *t* test (two-sided) or ANOVA for experiments with more than two subgroups. Post hoc range tests and pair wise multiple comparisons were performed with *t* test (two-sided) with Bonferroni adjustment. *P* values <0.05 were considered statistically significant. All analyses were performed with SPSS 11.5 (SPSS Inc.).

References

1. Isner, J.M. & Asahara, T. Angiogenesis and vasculogenesis as therapeutic strategies for postnatal neovascularization. *J Clin Invest* **103**, 1231-6 (1999).
2. Folkman, J. Angiogenesis in cancer, vascular, rheumatoid and other disease. *Nat Med* **1**, 27-31 (1995).
3. Risau, W. Mechanisms of angiogenesis. *Nature* **386**, 671-4. (1997).
4. Carmeliet, P. & Jain, R.K. Angiogenesis in cancer and other diseases. *Nature* **407**, 249-57. (2000).
5. Asahara, T. *et al.* Isolation of putative progenitor endothelial cells for angiogenesis. *Science* **275**, 964-7. (1997).
6. Shi, Q. *et al.* Evidence for circulating bone marrow-derived endothelial cells. *Blood* **92**, 362-7. (1998).
7. Kalka, C. *et al.* Transplantation of ex vivo expanded endothelial progenitor cells for therapeutic neovascularization. *Proc Natl Acad Sci U S A* **97**, 3422-7. (2000).
8. Kawamoto, A. *et al.* Therapeutic potential of ex vivo expanded endothelial progenitor cells for myocardial ischemia. *Circulation* **103**, 634-7. (2001).
9. Assmus, B. *et al.* Transplantation of Progenitor Cells and Regeneration Enhancement in Acute Myocardial Infarction (TOPCARE-AMI). *Circulation* **106**, 3009-17. (2002).
10. Dimmeler, S. *et al.* HMG-CoA reductase inhibitors (statins) increase endothelial progenitor cells via the PI 3-kinase/Akt pathway. *J Clin Invest* **108**, 391-7. (2001).
11. Vasa, M. *et al.* Number and migratory activity of circulating endothelial progenitor cells inversely correlate with risk factors for coronary artery disease. *Circ Res* **89**, E1-7. (2001).
12. Dunn, B.M. Structure and mechanism of the pepsin-like family of aspartic peptidases. *Chem Rev* **102**, 4431-58. (2002).
13. Turk, V., Turk, B. & Turk, D. Lysosomal cysteine proteases: facts and opportunities. *Embo J* **20**, 4629-33. (2001).
14. Lah, T.T. & Kos, J. Cysteine proteinases in cancer progression and their clinical relevance for prognosis. *Biol Chem* **379**, 125-30. (1998).
15. Berchem, G. *et al.* Cathepsin-D affects multiple tumor progression steps in vivo: proliferation, angiogenesis and apoptosis. *Oncogene* **21**, 5951-5. (2002).
16. Krueger, S., Kellner, U., Buehling, F. & Roessner, A. Cathepsin L antisense oligonucleotides in a human osteosarcoma cell line: effects on the invasive phenotype. *Cancer Gene Ther* **8**, 522-8. (2001).
17. Mason, R.W., Gal, S. & Gottesman, M.M. The identification of the major excreted protein (MEP) from a transformed mouse fibroblast cell line as a catalytically active precursor form of cathepsin L. *Biochem J* **248**, 449-54. (1987).
18. Hanahan, D. & Folkman, J. Patterns and emerging mechanisms of the angiogenic switch during tumorigenesis. *Cell* **86**, 353-64. (1996).

19. Honey, K., Nakagawa, T., Peters, C. & Rudensky, A. Cathepsin L regulates CD4+ T cell selection independently of its effect on invariant chain: a role in the generation of positively selecting peptide ligands. *J Exp Med* **195**, 1349-58. (2002).
20. Nakagawa, T. *et al.* Cathepsin L: critical role in Ii degradation and CD4 T cell selection in the thymus. *Science* **280**, 450-3. (1998).
21. Roth, W. *et al.* Cathepsin L deficiency as molecular defect of furless: hyperproliferation of keratinocytes and pertubation of hair follicle cycling. *Faseb J* **14**, 2075-86. (2000).
22. Tobin, D.J. *et al.* The lysosomal protease cathepsin L is an important regulator of keratinocyte and melanocyte differentiation during hair follicle morphogenesis and cycling. *Am J Pathol* **160**, 1807-21. (2002).
23. Stypmann, J. *et al.* Dilated cardiomyopathy in mice deficient for the lysosomal cysteine peptidase cathepsin L. *Proc Natl Acad Sci U S A* **99**, 6234-9. (2002).
24. Fiebiger, E. *et al.* Invariant chain controls the activity of extracellular cathepsin L. *J Exp Med* **196**, 1263-9. (2002).
25. Stack, M.S., Gately, S., Bafetti, L.M., Enghild, J.J. & Soff, G.A. Angiostatin inhibits endothelial and melanoma cellular invasion by blocking matrix-enhanced plasminogen activation. *Biochem J* **340**, 77-84. (1999).
26. Taraboletti, G. *et al.* Shedding of the matrix metalloproteinases MMP-2, MMP-9, and MT1-MMP as membrane vesicle-associated components by endothelial cells. *Am J Pathol* **160**, 673-80. (2002).
27. Walker, B., Lynas, J.F., Meighan, M.A. & Bromme, D. Evaluation of dipeptide alpha-keto-beta-aldehydes as new inhibitors of cathepsin S. *Biochem Biophys Res Commun* **275**, 401-5. (2000).
28. Li, Z. *et al.* Regulation of collagenase activities of human cathepsins by glycosaminoglycans. *J Biol Chem* **26**, 26 (2003).
29. Heymans, S. *et al.* Inhibition of plasminogen activators or matrix metalloproteinases prevents cardiac rupture but impairs therapeutic angiogenesis and causes cardiac failure. *Nat Med* **5**, 1135-42. (1999).
30. Libby, P. & Schonbeck, U. Drilling for oxygen: angiogenesis involves proteolysis of the extracellular matrix. *Circ Res* **89**, 195-7. (2001).
31. Carmeliet, P. Mechanisms of angiogenesis and arteriogenesis. *Nat Med* **6**, 389-95. (2000).
32. Devy, L. *et al.* The pro- or antiangiogenic effect of plasminogen activator inhibitor 1 is dose dependent. *Faseb J* **16**, 147-54. (2002).
33. Rooprai, H.K. & McCormick, D. Proteases and their inhibitors in human brain tumours: a review. *Anticancer Res* **17**, 4151-62. (1997).
34. Shi, G.P. *et al.* Deficiency of the cysteine protease cathepsin S impairs microvessel growth. *Circ Res* **92**, 493-500. (2003).
35. Morikawa, W. *et al.* Angiostatin generation by cathepsin D secreted by human prostate carcinoma cells. *J Biol Chem* **275**, 38912-20. (2000).

36. Felbor, U. *et al.* Secreted cathepsin L generates endostatin from collagen XVIII. *Embo J* **19**, 1187-94. (2000).
37. Lyden, D. *et al.* Impaired recruitment of bone-marrow-derived endothelial and hematopoietic precursor cells blocks tumor angiogenesis and growth. *Nat Med* **7**, 1194-201. (2001).
38. Rafii, S., Lyden, D., Benezra, R., Hattori, K. & Heissig, B. Vascular and haematopoietic stem cells: novel targets for anti-angiogenesis therapy? *Nat Rev Cancer* **2**, 826-35. (2002).
39. Houseweart, M.K. *et al.* Cathepsin B but not cathepsins L or S contributes to the pathogenesis of Unverricht-Lundborg progressive myoclonus epilepsy (EPM1). *J Neurobiol* **56**, 315-27. (2003).
40. Saftig, P. *et al.* Mice deficient for the lysosomal proteinase cathepsin D exhibit progressive atrophy of the intestinal mucosa and profound destruction of lymphoid cells. *Embo J* **14**, 3599-608. (1995).
41. Lelongt, B. *et al.* Matrix metalloproteinase 9 protects mice from anti-glomerular basement membrane nephritis through its fibrinolytic activity. *J Exp Med* **193**, 793-802. (2001).
42. Urbich, C. *et al.* Shear stress-induced endothelial cell migration involves integrin signaling via the fibronectin receptor subunits alpha(5) and beta(1). *Arterioscler Thromb Vasc Biol* **22**, 69-75. (2002).
43. Hoffmann, J. *et al.* Aging enhances the sensitivity of endothelial cells toward apoptotic stimuli: important role of nitric oxide. *Circ Res* **89**, 709-15. (2001).
44. Hofmann, W.K. *et al.* Characterization of gene expression of CD34+ cells from normal and myelodysplastic bone marrow. *Blood* **100**, 3553-60. (2002).
45. Kamboj, R.C., Pal, S., Raghav, N. & Singh, H. A selective colorimetric assay for cathepsin L using Z-Phe-Arg-4-methoxy-beta-naphthylamide. *Biochimie* **75**, 873-8. (1993).
46. Ebert, D.H., Deussing, J., Peters, C. & Dermody, T.S. Cathepsin L and cathepsin B mediate reovirus disassembly in murine fibroblast cells. *J Biol Chem* **277**, 24609-17. (2002).
47. Urbich, C. *et al.* Dephosphorylation of endothelial nitric oxide synthase contributes to the anti-angiogenic effects of endostatin. *Faseb J* **16**, 706-8. (2002).
48. Aicher, A. *et al.* Essential role of endothelial nitric oxide synthase for mobilization of stem and progenitor cells. *Nat Med* **9**, 1370-6. (2003).
49. Dennhofer, R. *et al.* Invasion of melanoma cells into dermal connective tissue in vitro: evidence for an important role of cysteine proteases. *Int J Cancer* **106**, 316-23. (2003).
50. Kaberdin, V.R. & McDowall, K.J. Expanding the use of zymography by the chemical linkage of small, defined substrates to the gel matrix. *Genome Res* **13**, 1961-5. (2003).
51. Hinds, K.A. *et al.* Highly efficient endosomal labeling of progenitor and stem cells with large magnetic particles allows magnetic resonance imaging of single cells. *Blood* **3**, 3 (2003).

Figure legends

Figure 1: Gene expression analysis of EPCs and HUVECs

a, Expression of endothelial marker proteins in EPCs (left panel) and HUVECs (right panel) was measured by FACS analysis. Staining of KDR, CD105 and VE-cadherin (bold lines) is shown compared to isotype controls (dotted lines). Representative images out of at least 3 independent experiments are shown. ***b,*** PBS, HUVEC or EPC (each $8x10^5$ cells; *n*=5) were injected into a murine model of hind limb ischemia. Results are shown as box plots representing median 25^{th} and 75^{th} percentiles as boxes and 5^{th} and 95^{th} percentiles as whiskers. **P*<0.001 versus PBS, ***P*<0.001 versus EPCs. ***c,*** Total RNA of EPCs, HUVECs and $CD14^+$ monocytes (each *n*=3) was isolated and the gene expression profile was assessed with the Affymetrix gene chip expression assay. A gene tree analysis is shown. The colour scale is shown on the right. The brightness indicates the trust. Blue colour indicates low expression, red colour indicates high expression. Expression of prominent clusters is marked on the right side. ***d,*** The mRNA expression (normalized data) of various cathepsins and cystatins in HUVECs, EPCs and monocytes is summarized. Data are mean ± SEM, *n*=3; **P*<0.05 versus HUVEC.

Figure 2: The expression and activity of cathepsin L is increased in EPCs

a-d**,** HUVECs, EPCs and $CD14^+$ monocytes were lyzed and the protein expression of CathD ***(a)*** or CathL ***(c)*** was analyzed by Western blot. Tubulin serves as loading control. A representative blot out of 4 independent experiments is shown. ***b/d*****,** Blots were scanned and protein expression was quantified by densitometric analysis. The ratio for CathD/tubulin ***(b)*** or CathL/tubulin ***(d)*** is shown. Data are mean ± SEM, *n*=4; **P*<0.05 versus HUVEC. ***e/f,*** HUVECs, EPCs, $CD14^+$ monocytes or HMVECs were lyzed and the amount of CathD ***(e)*** or CathL ***(f)*** was measured by immunoassay. Data are mean ± SEM, *n*=4; **P*<0.05 versus HUVEC. ***g,*** CathL activity was measured in HUVECs, EPCs or $CD14^+$ monocytes using the fluorogenic substrate Z-Phe-Arg-4-methoxy-ß-naphthylamide-hydrochloride (50 µM). Data are mean ± SEM, *n*=4; **P*<0.05 versus HUVEC. ***h***, The mRNA expression of p41 was measured by RT-PCR. A representative gel electrophoresis is shown. GAPDH serves as control. Data are mean ± SEM, *n*=3 (right panel).

Figure 3: Role of CathL for neovascularization

a, $CathL^{+/+}$, $CathL^{+/-}$ or $CathL^{-/-}$ mice were subjected to a model of hind limb ischemia. After two weeks, ischemic (right)/normal (left) limb blood flow ratio was measured with a laser

Doppler blood flow meter. Results are shown as box plots representing median 25th and 75th percentiles as boxes and 5th and 95th percentiles as whiskers. *n*=3, *p<0.05 vs. wt. ***b,*** Schematic illustration of the multi-step process of vasculogenesis. ***c,*** EPCs were detached at day 4, labeled with CellTracker green CMFDA and plated on fibronectin, collagen or laminin-coated dishes for 40 min. Plates were washed and adherent cells were counted. Data are mean ± SEM, *n*=5. ***d*****,** Reendothelialization by EPCs was determined as described in the method section. Attachment and homing of EPCs to previously denuded arterial segments was assessed by cryosections stained for the endothelial marker von Willebrand factor (green) and SYTOX (blue). ***e,*** the number of incorporated EPCs (CM-Dil positive, red) per section was assessed. A total of three sections per rat were analyzed. Data are mean ± SEM, *n*=6. ***f*****,** proliferation of flk-1^{+} bone marrow-derived cells or human EPCs that were either untreated or pretreated with Z-FF-FMK (10 µM; 2h) was measured by FACS analysis after pulsing with BrdU and staining with BrdU-FITC or BrdU ELISA. Data are mean ± SEM (% of control or wt, respectively), *n*=3-4. Apoptosis of sca-1^{+}/flk-1^{+} bone marrow-derived cells cells or human EPCs that were either untreated or pretreated with Z-FF-FMK (10 µM; 2h) was assessed by FACS analysis after staining with annexin-PE. Data are mean ± SEM (% of control or wt, respectively), *n*=5. For determination of migration, sca-1^{+} bone marrow-derived cells or human EPCs that were either untreated or pretreated with Z-FF-FMK (10 µM; 2h) were placed in a modified Boyden chamber. Data are mean ± SEM (% of control or wt, respectively), *n*=4-5.

Figure 4: Role of CathL for EPC invasion

a, In vitro invasion: a modified Boyden chamber was filled with 50 µl matrigel and 1x10^{5} cells were seeded in serum-free EBM medium in the upper compartment in the presence or absence of the inhibitors (cystatin C: 10 nM; CathL-inhibitor Z-FF-FMK: 10 µM; CathS-inhibitor Z-FL-COCHO: 10 µM) as indicated. After 24 h of incubation, the cells in the lower part of the chamber were stained with Dil-Ac-LDL. The invasion of EPCs, HUVECs and CD14^{+} monocytes was determined by two independent investigators (cells per high powerfield). Data are mean ± SEM, *n*=4, *P<0.05 versus HUVEC, $^{\#}$P<0.05 versus EPC. ***b,*** The invasion of sca-1^{+} bone marrow-derived cells of wt or CathL$^{-/-}$ mice was measured using a modified Boyden chamber filled with matrigel. Data are mean ± SEM (% of wt), n=3, *p<0.05. ***c*****,** Cell lysates of HUVECs or EPCs that were either untreated or pretreated with Z-FF-FMK (10 µM; 2h) were analyzed by modified gelatin or collagen zymography. Representative zymographies are shown. d, Densitometric quantification of the gelatin zymographies are shown. Data are mean ± SEM, *n*=4, *p<0.05 vs. HUVEC, $^{\#}$p<0.05 vs.

EPCs. ***e*,** Cell culture supernatants (SN, 10x) of EPCs that were either untreated or pretreated with Z-FF-FMK (10 µM; 2h) were analyzed by gelatin zymography for determination of MMP activity. A representative zymography is shown.

Figure 5: CathL is required for improvement of neovascularization

Human EPCs or human EPCs pretreated for 2 h with the CathL-inhibitor Z-FF-FMK ($8x10^5$ cells; each *n*=7-8) were injected into a murine model of hind limb ischemia. ***a,*** Representative laser Doppler images 2 weeks after induction of hind limb ischemia are shown. Arrows indicate the ischemic leg. ***b,*** Results are shown as box plots representing median 25^{th} and 75^{th} percentiles as boxes and 5^{th} and 95^{th} percentiles as whiskers. **P*<0.01 vs. EPC. ***c,*** Capillary density was determined in 8-µm frozen sections of the adductor and semimembraneous muscles. Endothelial cells were stained for CD31 (PE-labeled; BD Biosciences). Myocyte membranes were stained using an antibody to laminin (rabbit) followed by anti-rabbit-Alexa 488. Data are mean ± SEM, n=4. **P*<0.05 vs. PBS, ***P*<0.05 vs. EPC. ***d,*** Early EPC homing to the area of ischemia was investigated by magnetic resonance imaging. After 24 hours of ischemia, EPCs labeled with magnetic beads and pretreated with DMSO or the CathL-inhibitor Z-FF-FMK were injected. MRI scans were performed after another 24 hours. The TIRM images are shown in the upper panel. The white arrows indicate the area of ischemia. Enriched magnetically-labeled EPCs can be visualized as hypointense spots, which disappear in mice transplanted with CathL-inhibitor-pretreated EPCs. The greatest magnitude of changes related to the incorporation of superparamagnetic particles-loaded EPCs involved T2*-weighted images as shown in the lower panel. The black arrows indicate an area of marked EPC enrichment. ***e,*** Histological sections were obtained 2 weeks after induction of ischemia. Endothelial cells were stained with CD146-FITC. Human EPCs were identified by co-staining for HLA-A,B,C-APC and CD146-FITC. ***f,*** Incorporation of EPCs was quantified and results are shown as box plots representing median 25^{th} and 75^{th} percentiles as boxes and 5^{th} and 95^{th} percentiles as whiskers. **P*<0.05 vs. EPC, ***P*<0.01 vs. EPC. ***g,*** Bone marrow cells (BMC) from wild-type (wt), $CathL^{-/-}$, $CathD^{-/-}$ or $MMP\text{-}9^{-/-}$ mice (10^6 cells; each *n*=4-6) were isolated and injected into a murine model of hind limb ischemia. Laser Doppler images were quantified as box plots representing median 25^{th} and 75^{th} percentiles as boxes and 5^{th} and 95^{th} percentiles as whiskers (right panel).

Figure 6: Overexpression of CathL in mature endothelial cells partially rescued the impaired improvement of neovascularization

HUVEC were transfected with an empty vector or human pro-CathL for 24 h. ***a***, The cells ($1.5x10^6$ cells; each *n*=4-5) were injected into a murine model of hind limb ischemia. Laser Doppler-derived relative blood flow was measured two weeks after induction of hind limb

ischemia. Results are shown as box plots representing median 25th and 75th percentiles as boxes and 5th and 95th percentiles as whiskers. *P<0.05 vs. vector-transfected cells. ***b,*** Transfected HUVEC were lyzed and expression of overexpressed CathL was detected by Western blot analysis. Tubulin serves as loading control. ***c***, Cells were lyzed and CathL activity was measured using the fluorogenic substrate Z-Phe-Arg-4-methoxy-ß-naphthylamide-hydrochloride (50 µM). Data are mean ± SEM (% of vector-transfected cells), n=3. ***d***, In vitro invasion was determined in a modified Boyden chamber filled with matrigel. Data are mean ± SEM (% of vector-transfected cells), n=3.

Figure 1: Urbich et al.

NMED-LA16306B

a

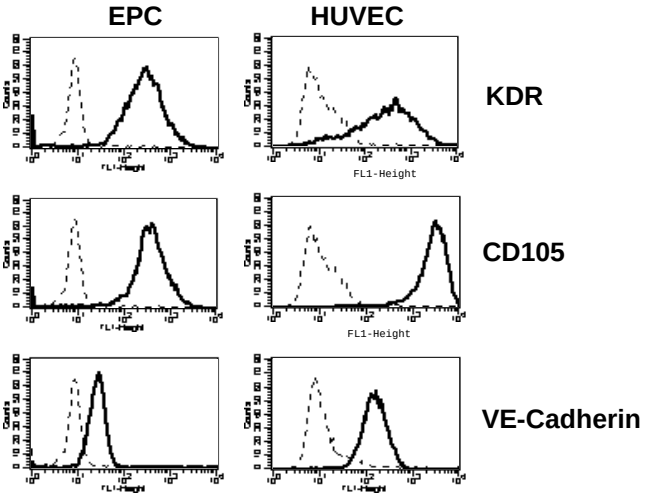

b

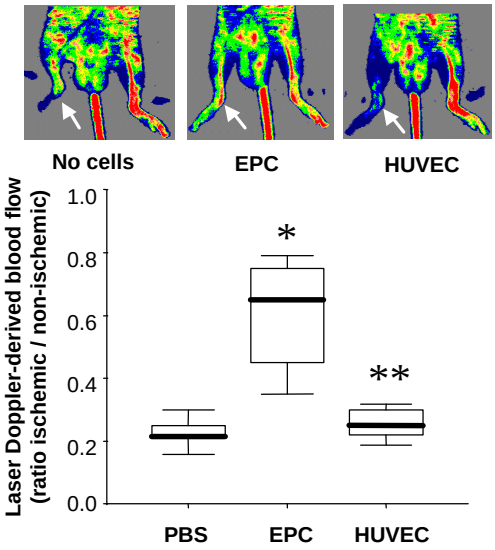

c

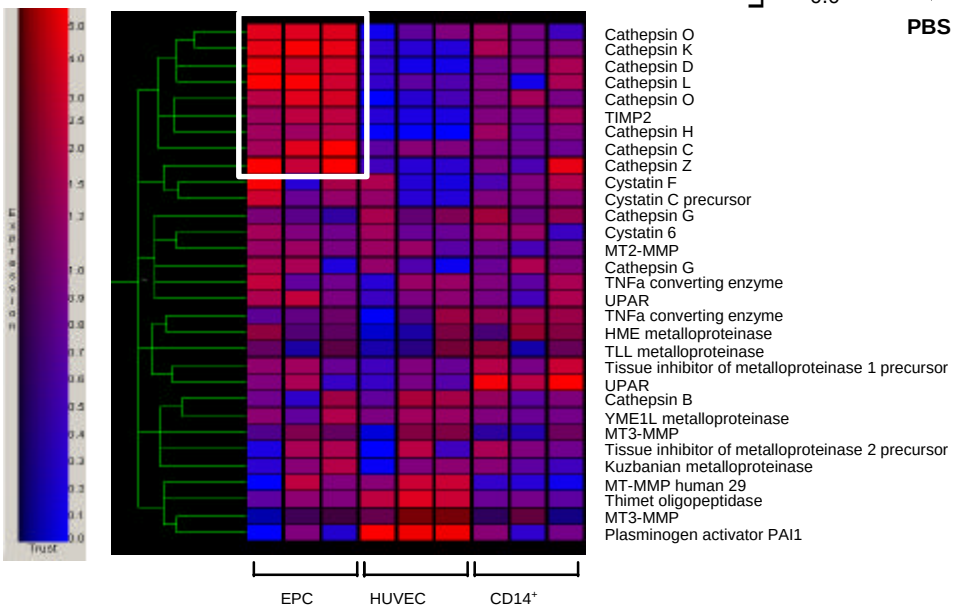

d

mRNA expression	Accession	EPC	HUVEC	CD14$^+$ monocytes
Cathepsin B	L22569	1.03±0.41	1.61±0.44	1.01±0.17
Cathepsin C	X87212	3.77±1.29	0.92±0.1	0.91±0.03
Cathepsin D	M63138	4.01±0.74*	0.22±0.07	1.15±0.19
Cathepsin E precursor	J05036	1.03±0.53	0.77±0.4	2.17±1.44
Cathepsin E	M84424	0.88±0.57	0.61±0.31	1.89±0.51
Cathepsin F	AF071748	2.32±0.75	1.15±0.63	0.56±0.17
Prepro-Cathepsin G	M16117	0.75±0.15	1.28±0.23	1.48±0.35
Cathepsin G	J04990	1.15±0.44	0.62±0.3	1.15±0.26
Prepro-Cathepsin H	X16832	1.53±0.21*	0.02±0.01	1.02±0.15
Pro-Cathepsin L	X12451	5.14±1.11*	0.6±0.1	0.92±0.42
Cathepsin O	X82153	4.03±0.07*	0.63±0.26	0.9±0.22
Cathepsin S	M90696	1.6±0.72	0.03±0.02	1.32±0.16
Cathepsin V	AB001928	4.4±2.32	1.28±0.83	2.6±1.8
Cathepsin W	AF013611	0.97±0.36	0.57±0.28	1.34±0.15
Cathepsin Z precursor	AF032906	6.32±2.01	0.39±0.06	2.05±1.25
Cystatin 1 precursor	J03870	0.64±0.32	2.26±1.67	1.42±0.23
Cystatin 6	N80906	1.1±0.17	1.0±0.18	0.98±0.25
Cystatin B	U46692	2.24±0.19*	0.92±0.11	0.85±0.04
Cystatin C precursor	AI362017	1.63±0.64	0.58±0.28	1.0±0.02
Cystatin D	X70377	0.47±0.26	1.18±0.61	1.63±0.38
Cystatin F (Leukocystatin)	AF031824	2.63±1.65	0.71±0.48	1.12±0.33
MT2-MMP	D86331	1.17±0.09	1.07±0.19	0.8±0.12
MT3-MMP	D83646	0.83±0.49	1.78±1.31	1.33±0.36
MMP-20	Y12779	0.73±0.39	2.15±1.76	1.55±0.32
UPAR	X74039	1.7±0.42	0.84±0.18	1.03±0.31
Plasminogen activator-1	J03764	0.43±0.3	164.89±44.04	0.78±0.2

Figure 2: Urbich et al.

NMED-LA16306B

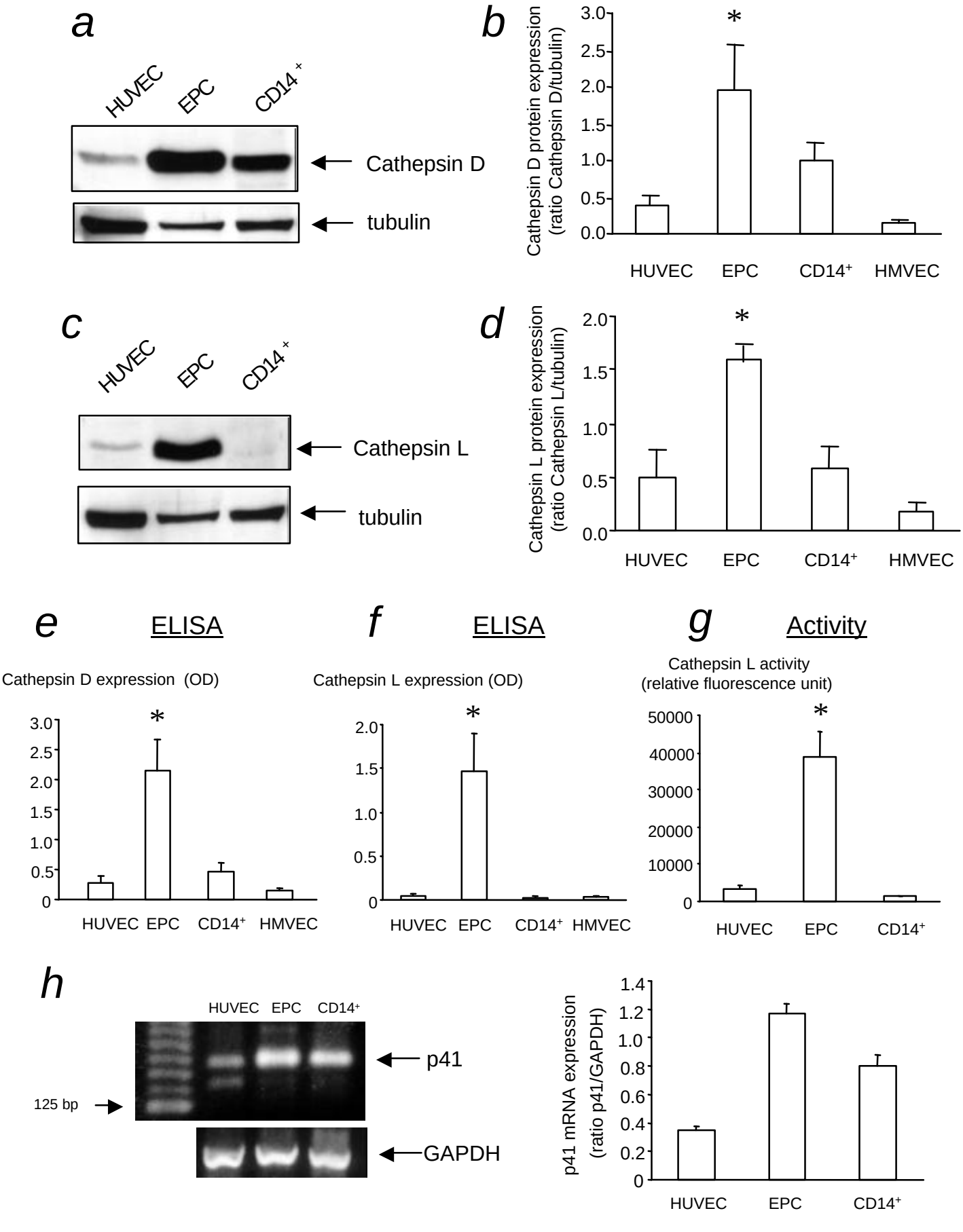

Figure 3: Urbich et al.

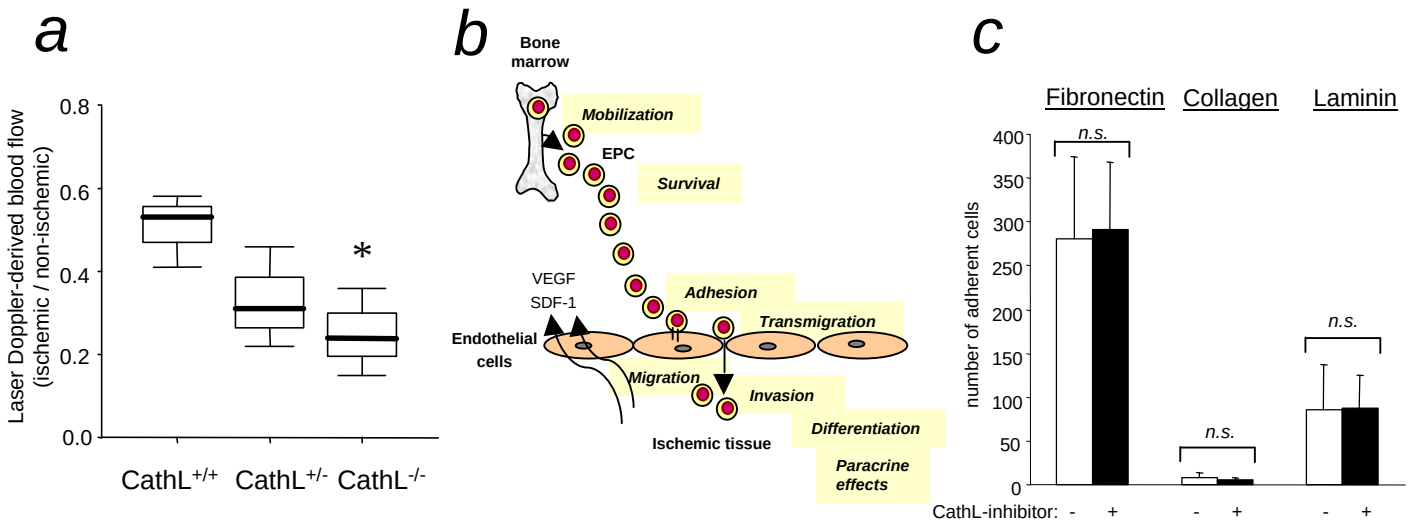

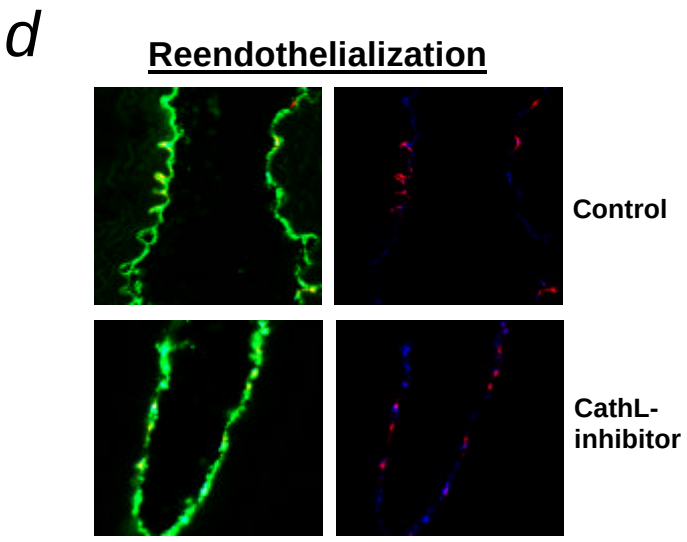

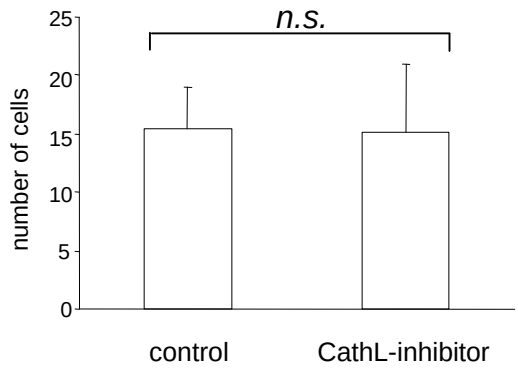

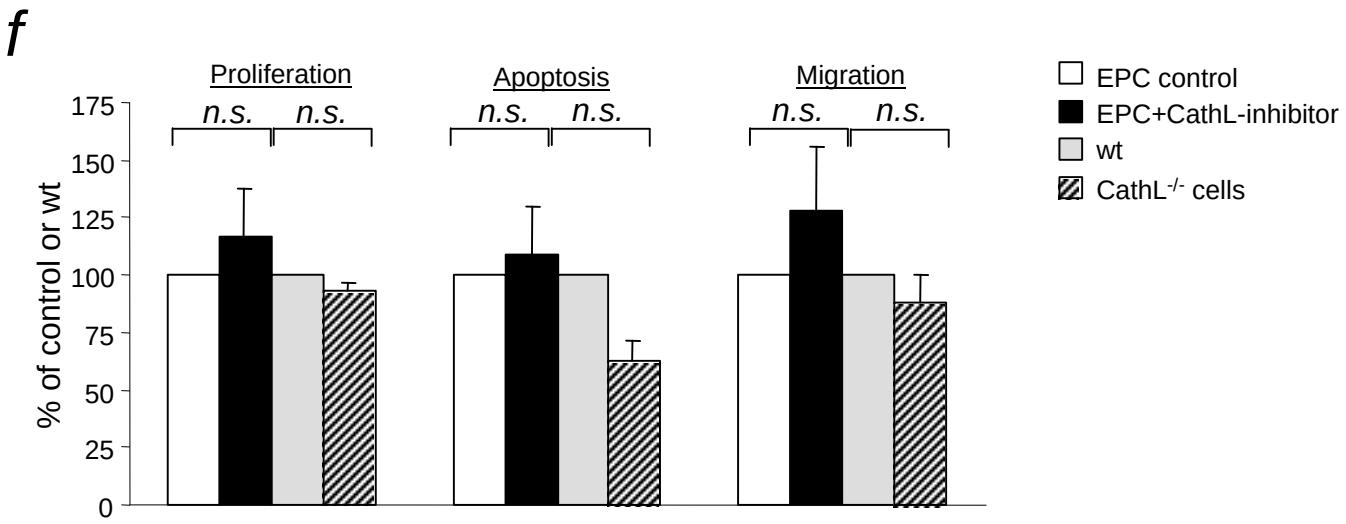

Figure 4: Urbich et al.

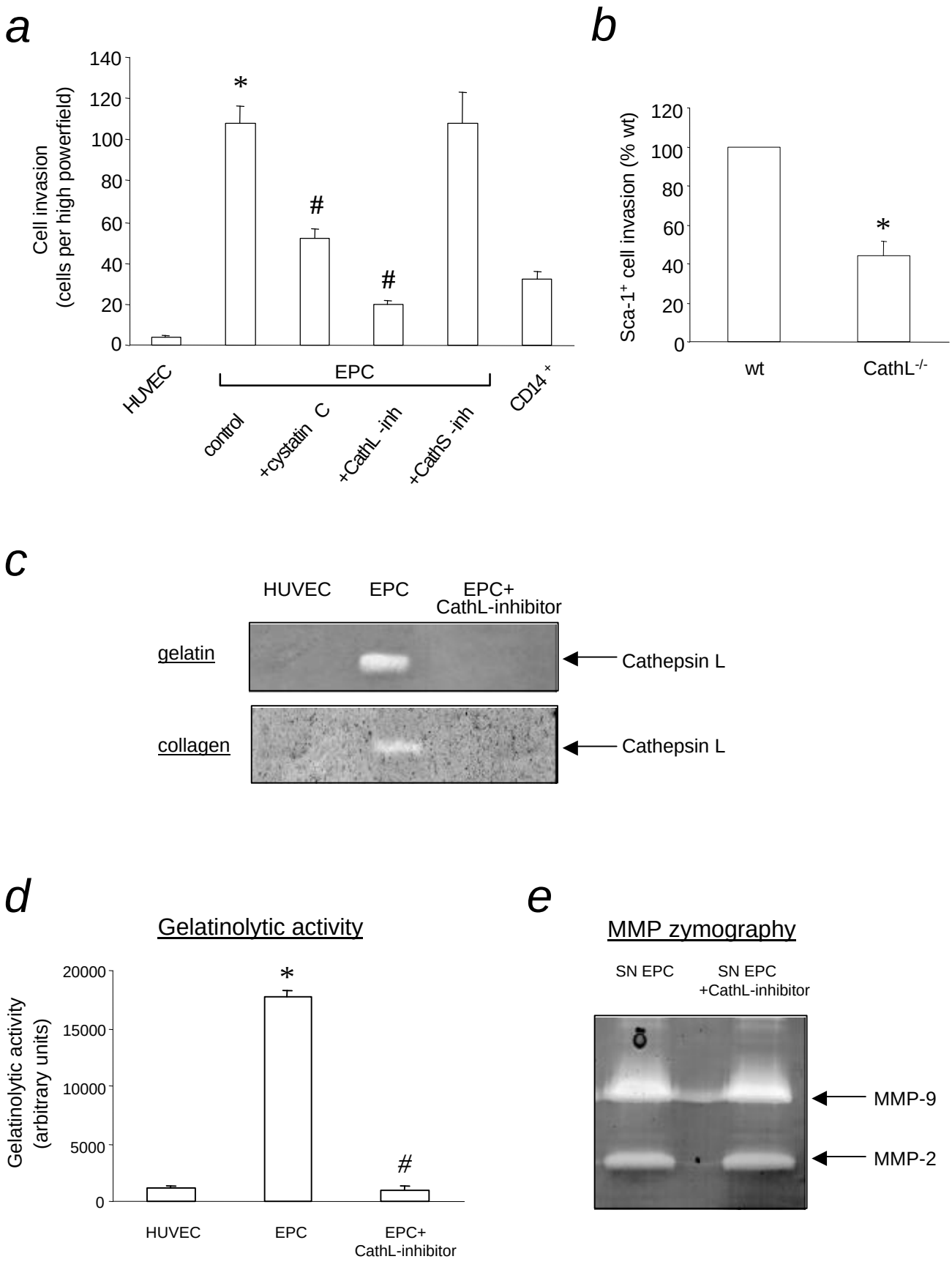

Figure 5: Urbich et al.

NMED-LA16306B

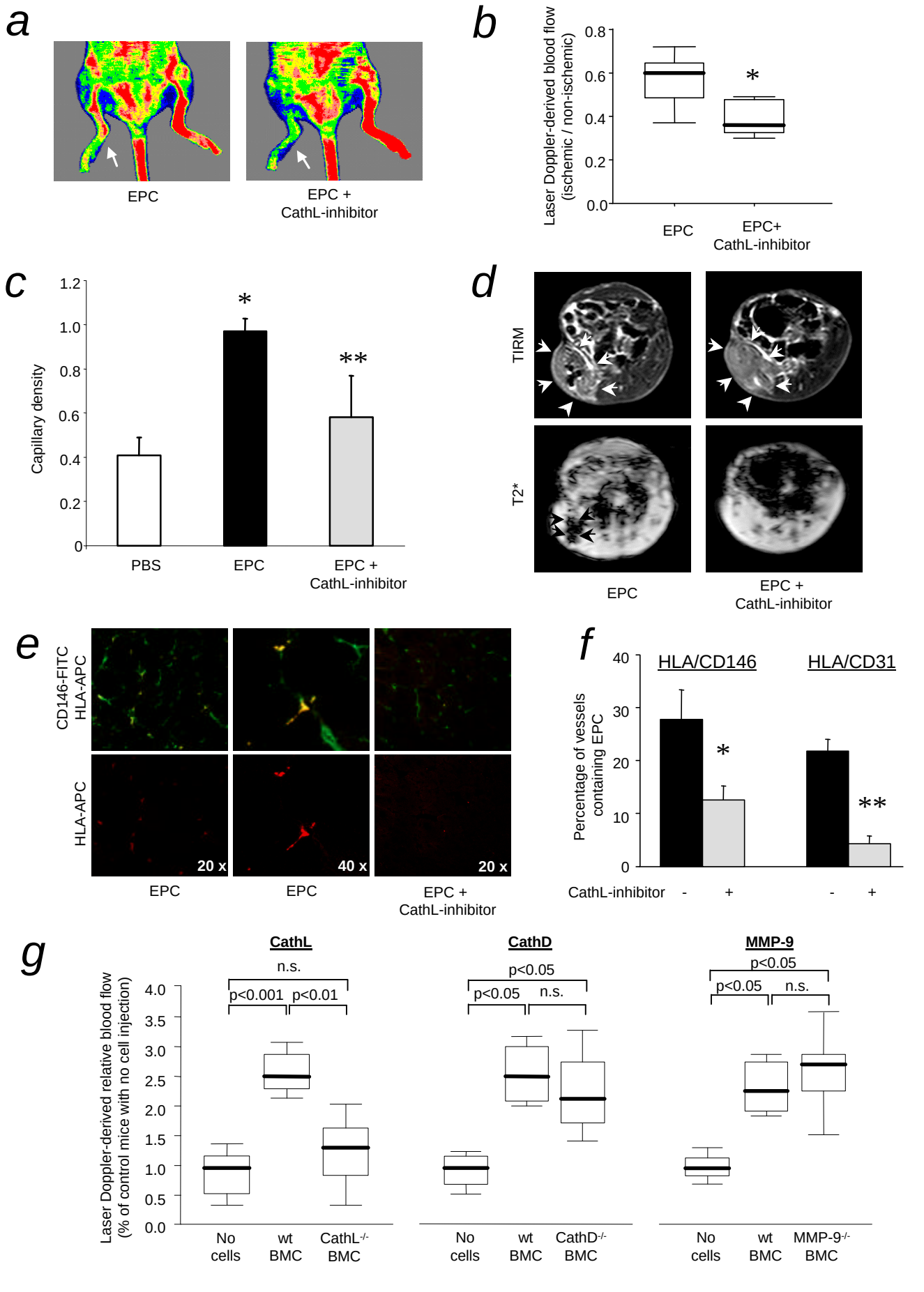

Figure 6:

a

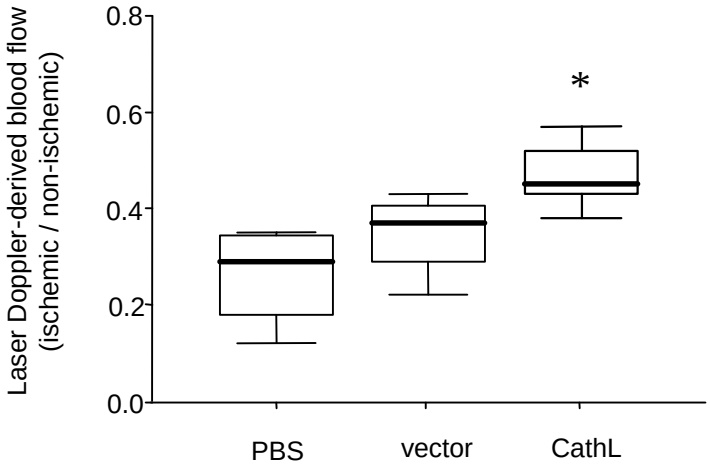

b

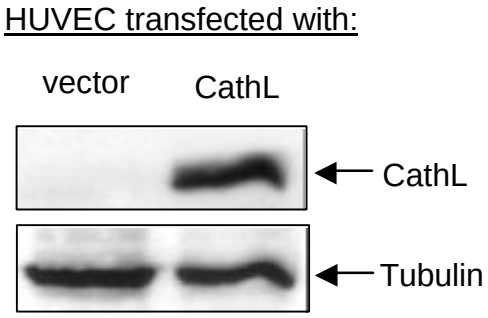

c

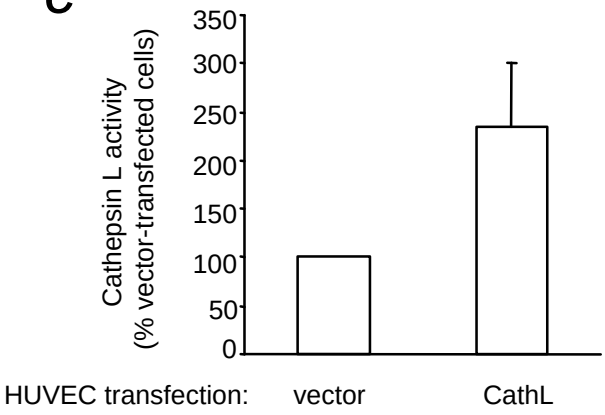

d

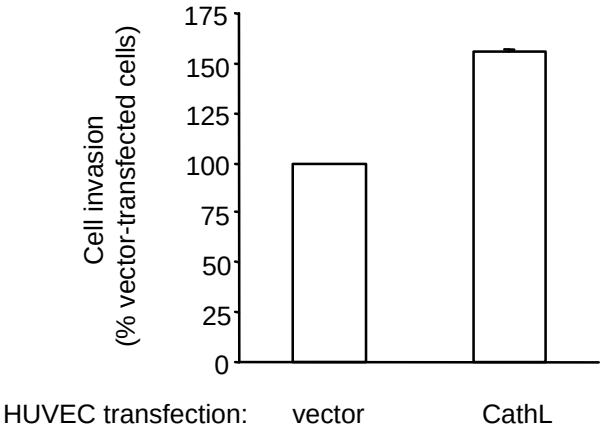

Supplementary figure 1

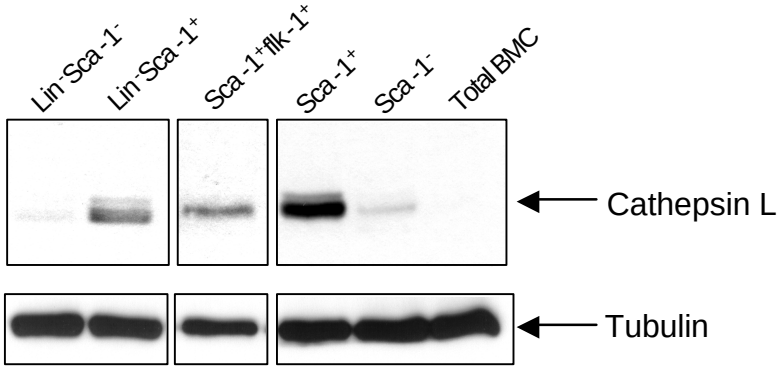

***Supplementary figure 1*,** Sca-1^{+} cells were purified from total bone marrow cells (BMC) using positive selection with anti-Sca-1- microbeads (Miltenyi Biotec, Bergisch-Gladbach, Germany). Lineage (Lin)$^{-}$ cells were purified from total bone marrow cells using negative depletion with anti-lineage-microbeads (Miltenyi Biotec, Bergisch-Gladbach, Germany). Sca-1^{+} cells were subsequently purified by FACS sorting of flk-1^{+} cells. Purity assessed by FACS analysis was >95%. Cells were lyzed and the protein expression of CathL was analyzed by Western blot. Tubulin serves as loading control. Representative blots are shown.

Supplementary figure 2

NMED-LA16306B

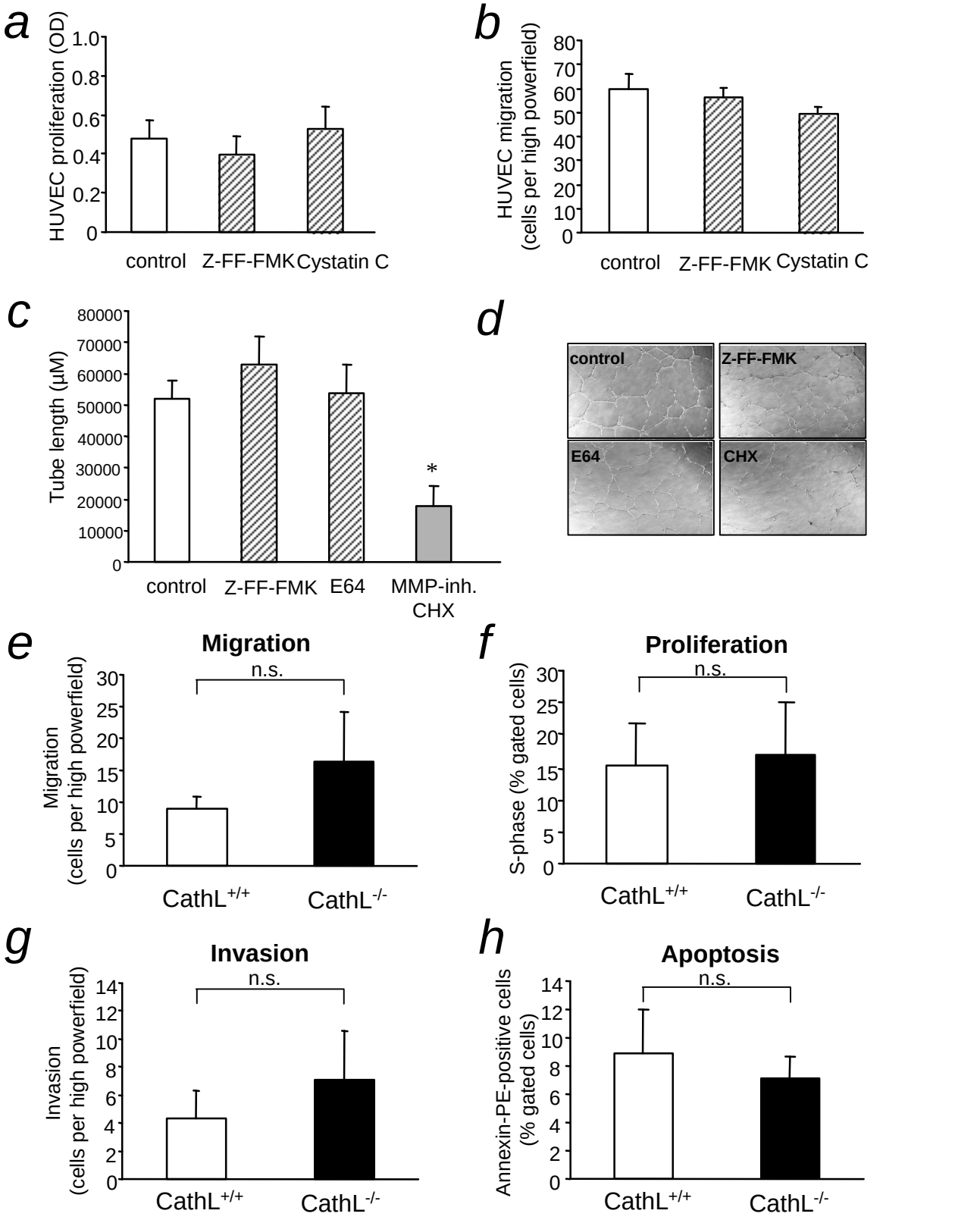

Supplementary figure 2 a-d, HUVECs were incubated as indicated with Z-FF-FMK (10 µM), cystatin C (10 nM), E64 (10 µM) or chlorhexidine (CHX, 10 µM) for 24 h. ***a,*** Proliferation was measured by BrdU incorporation, ***b***, migration was assessed in a modified Boyden chamber and ***c,*** tube formation was detected in a matrigel assay; *p<0.05, n=3. ***d,*** Representative micrographs are shown for the tube formation assay. ***e-h,*** aortic endothelial cells were isolated from CathL$^{+/+}$ or CathL$^{-/-}$ mice. Migration ***(e)*** was measured using a modified Boyden chamber, proliferation ***(f)*** was assessed by FACS analysis of BrdU incorporation, invasion ***(g)*** was measured with a matrigel-filled modified Boyden chamber and apoptosis ***(h)*** was detected by staining with Annexin-PE and FACS analysis.

Supplementary figure 3

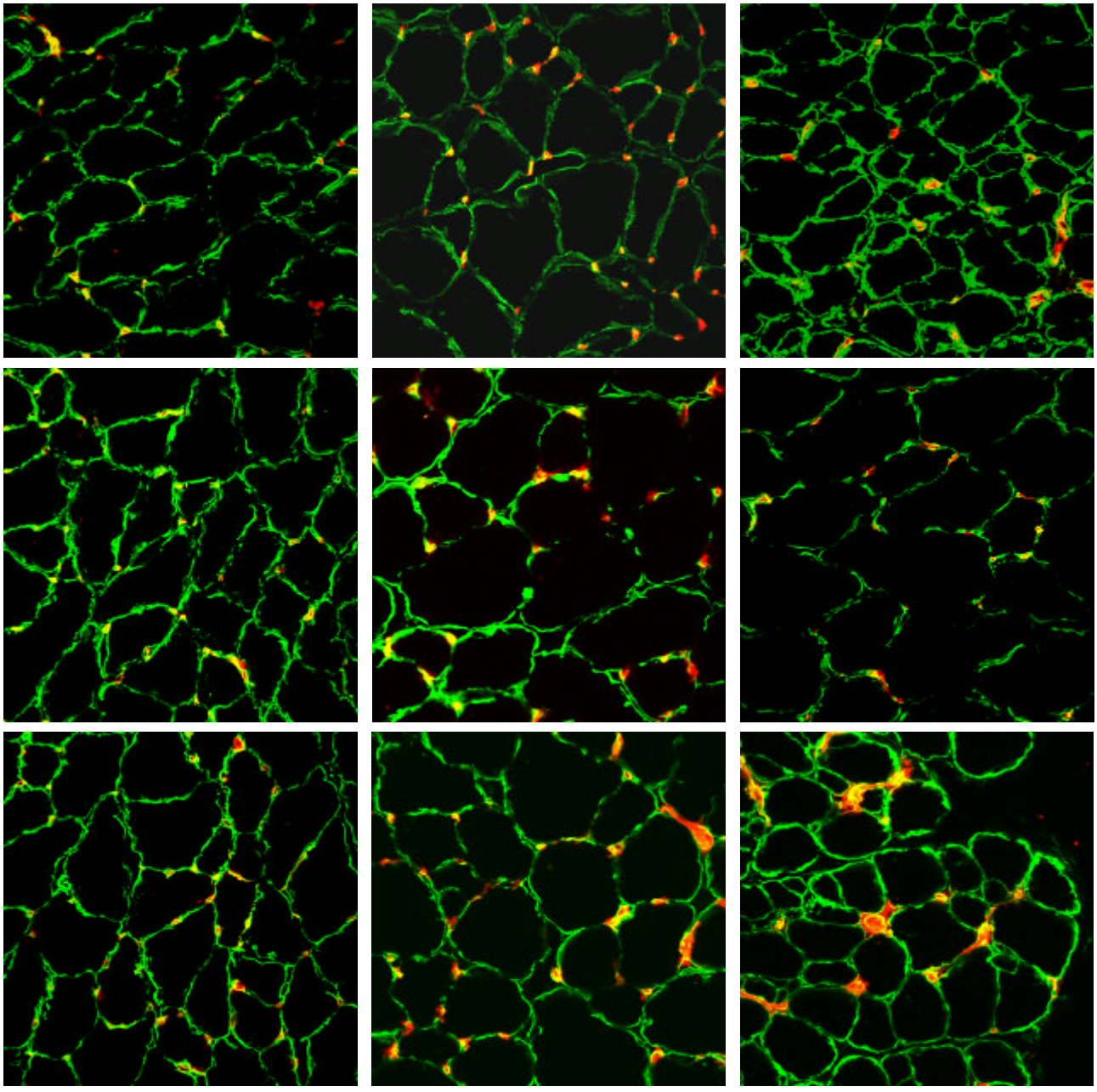

No cells EPC EPC + CathL-inhibitor

Supplementary figure 3, Capillary density was determined in 8-µm frozen sections of the adductor and semimembraneous muscles. Endothelial cells were stained for CD31 (PE-labeled; BD Biosciences, Heidelberg, Germany). For better identification, cell membranes of the myocytes were stained using an antibody to laminin (rabbit, abcam, Cambridge, UK) followed by anti-rabbit-Alexa 488. Three representative images of each treatment are shown.

Supplementary figure 4

NMED-LA16306B

a

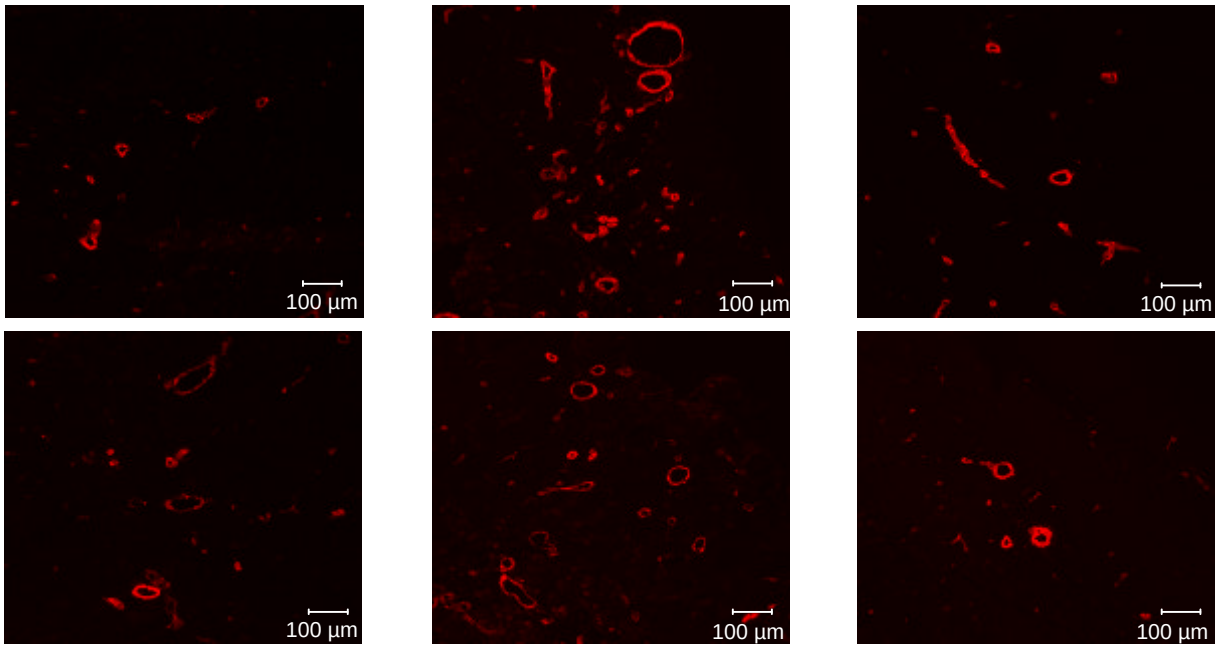

b

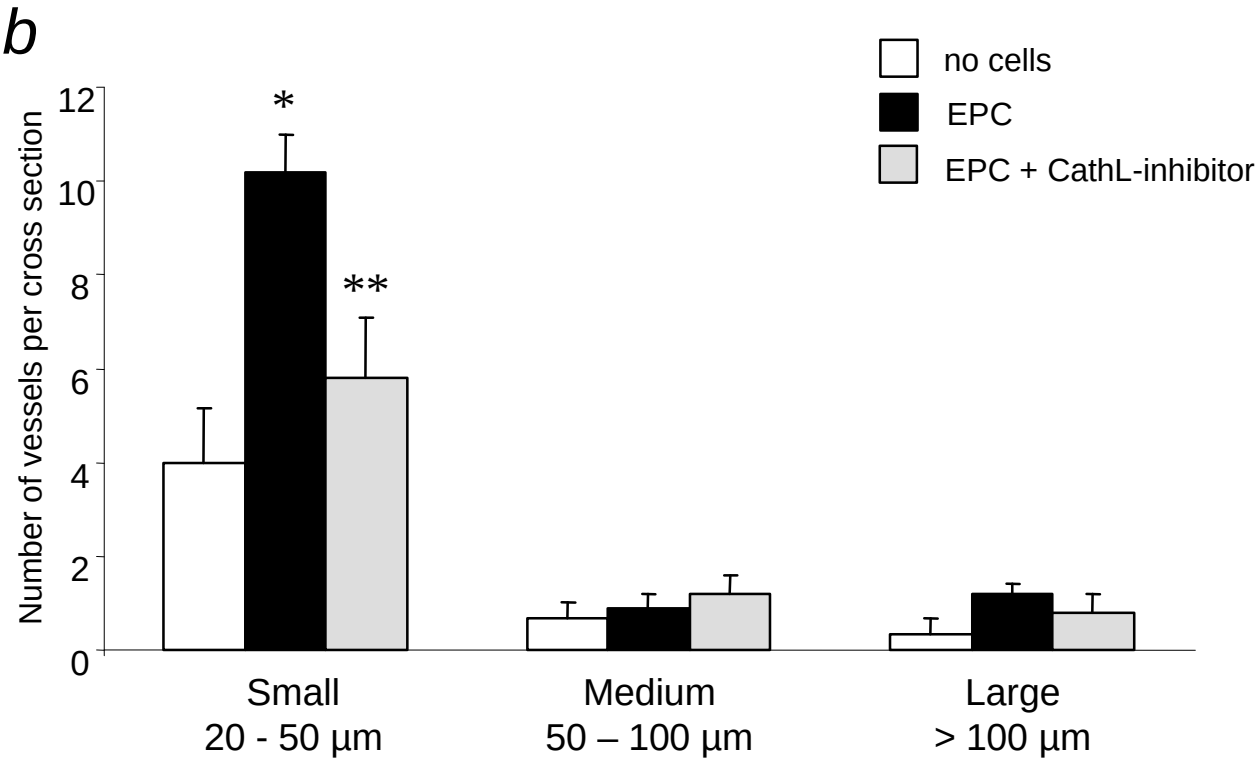

Supplementary figure 4 a,b, Conductance vessels in the adductor and semimembraneous muscles were identified by size (> 20 µm) and smooth muscle actin staining using a Cy3-labeled mouse monoclonal antibody for smooth muscle actin (Sigma). The number of small (<50 µm), medium (50 - 100 µm), and large vessels was counted separately. ***b****,* data are mean ± SEM, n=5, *p<0.05 vs. PBS, **p<0.05 vs. EPC.

Supplementary figure 5

High resolution images: incorporation of EPC

Example 1:

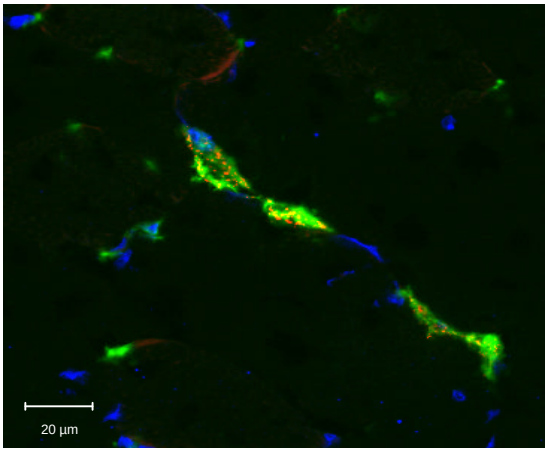

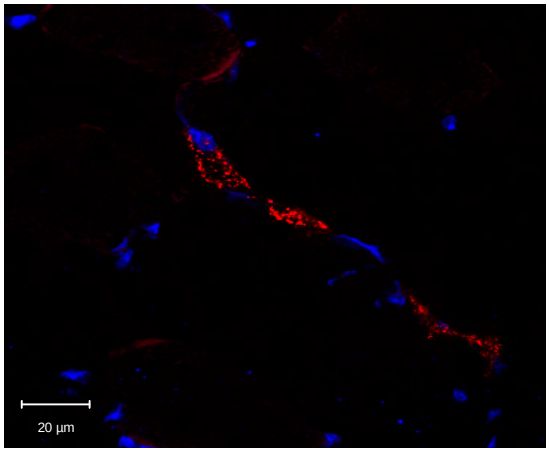

Example 2: Orthogonal sections

Y

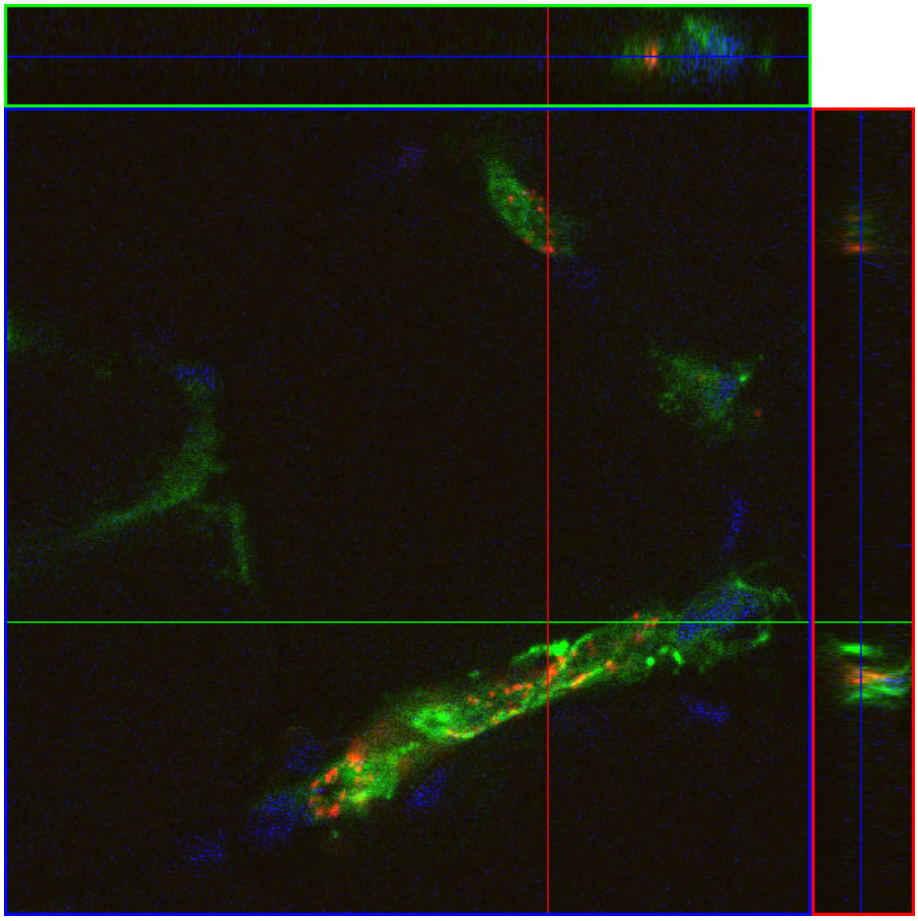

X

See movie file „supplementary movie 1 “

Red = CM-DIL
Green = vWF
Blue = Topro-3

Supplementary figure 5, Human EPCs ($8x10^5$ cells) were labeled with CM-Dil (Molecular probes, Portland, Oregon) and injected into nude mice 24 h after induction of hind limb ischemia. Histological sections were obtained 2 weeks after induction of ischemia. Endothelial cells were stained with von Willebrand-(vWF)-FITC (Acris Antibodies, Hiddenhausen, Germany). Nuclei were stained with Topro-3 (Molecular Probes). Incorporation of EPCs was detected by confocal microscopy. Representative images of two different examples are shown.

Supplementary figure 6

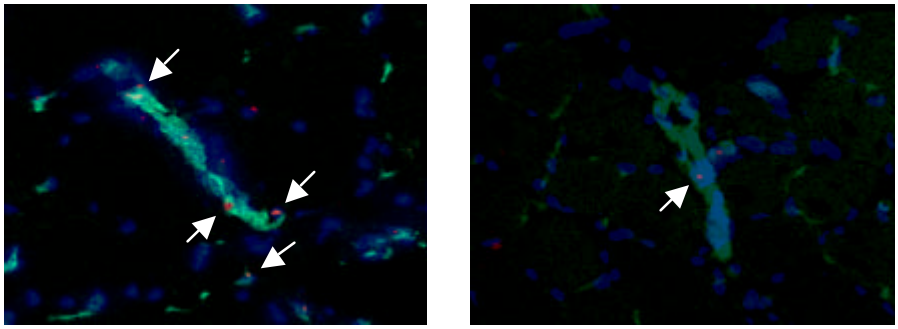

BMC wt BMC CathL$^{-/-}$

Supplementary figure 6, bone marrow cells (BMC) from male wild-type (wt) or CathL-deficient mice (10^6 cells; each n=5) were isolated and injected into female mice after induction of hind limb ischemia. Incorporated male murine EPCs were identified by FISH using probes against the murine Y-chromosome (PE-labeled; Vysis, Downers Grove, Illinois) according to Muller et al. (Circulation, 2002 Jul 2;106(1):31-5). Arrows indicate Y-chromosome-positive cells (red fluorescence). Endothelial cells were stained with CD31-FITC and nuclei were stained with 4',6-diamidine-2-phenylidole-dihydrochloride (DAPI, Roche Diagnostics).

Supplementary figure 7

NMED-LA16306B

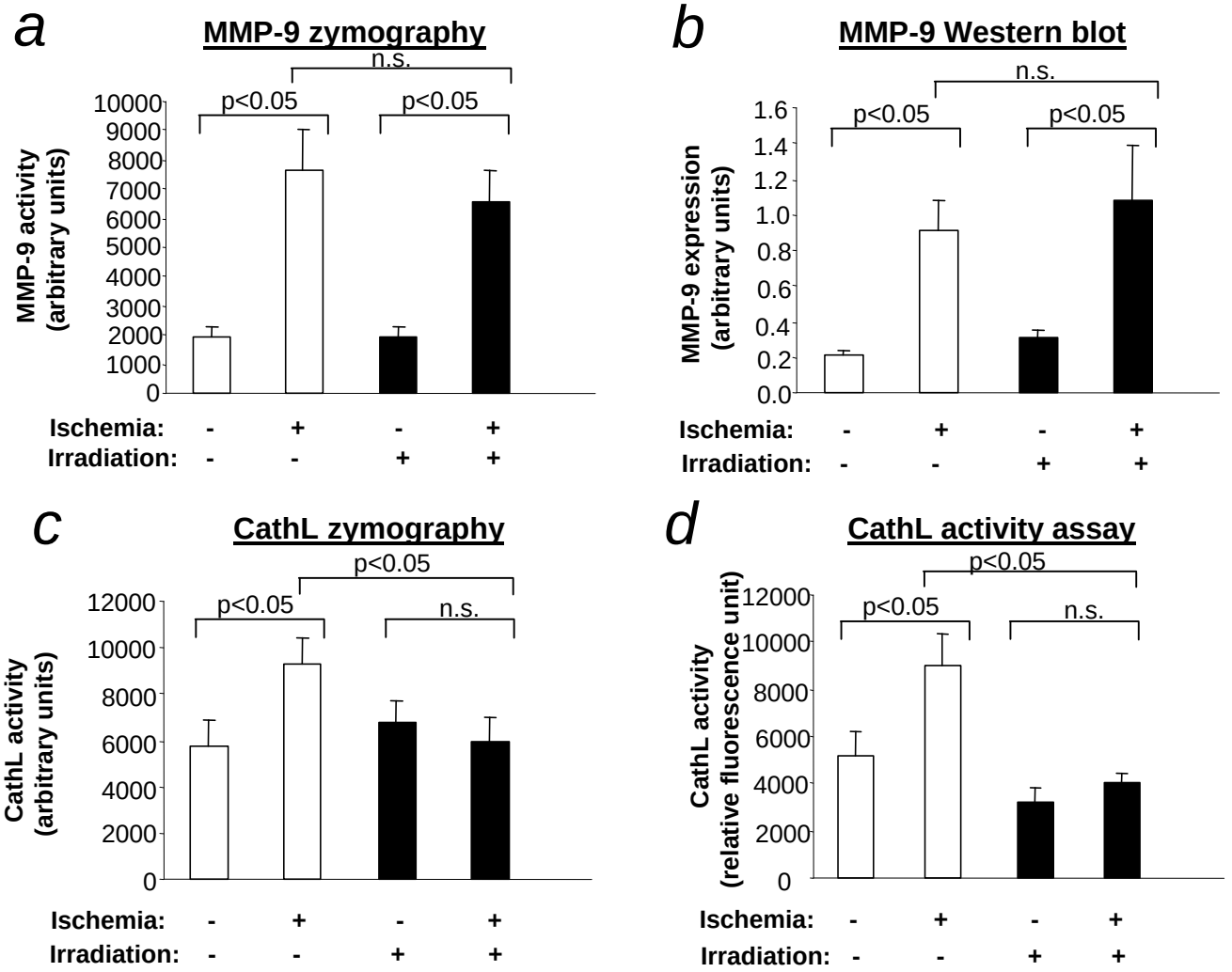

Supplementary figure 7: **MMP-9 and cathepsin L activity in ischemic tissues**

NMRI nude mice (The Jackson Laboratory, Bar Harbor, Maine) were either untreated or lethally irradiated once with 9.5 Gy. After 48 h, mice were subjected to unilateral induction of hind limb ischemia. Therefore, the proximal femoral artery including the superficial and the deep branches as well as the distal saphenous artery were ligated. After 48 h, animals were sacrificed and adductor and semimembraneous muscles were lyzed in buffer (1% Triton-X-100, 1 mM EDTA, 1mM EGTA, 150 mM NaCl, 1 mM PMSF, 20 mM Tris (pH 7.4), 2.5 mM Na-pyrophosphate, 1 mM ß-glycerolphosphate, 1 mM Na-orthovanadate, 1 µg/ml leupeptin) for 30 min at 4°C, followed by centrifugation (20000 x g, 15 min). The protein content of the samples was determined according to Bradford. Muscle lysates were used to measure MMP-9 or cathepsin L activity and MMP-9 expression.

Zymography

Metalloproteinase activity was analyzed by gelatinolytic zymography as described (Aicher et al., Nat Med. 2003 Nov;9(11):1370-6). Modified gelatin zymography for acidic proteases was performed according to Dennhöfer et al. (Int J Cancer. 2003 Sep 1;106(3):316-23). After gel electrophoresis, the gels were washed twice for 20 min with 25% isopropanol to remove SDS (Kaberdin et al., Genome Res. 2003 Aug;13(8):1961-5).

Western blot analysis

Blots were incubated with an antibody against MMP-9 (1:200, R&D Systems, Wiesbaden, Germany). Blots were reprobed with ERK1/2 (1:1000, Cell Signaling, Frankfurt, Germany). The autoradiographies were scanned and semiquantitatively analyzed.

CathL-activity assay

Lysates were incubated with the fluorogenic substrate Z-Phe-Arg-4-methoxy-ß-naphthylamide-hydrochloride (50 µM; Sigma) in the presence of 4 M urea at pH 4.7 (Kamboj et al., Biochimie. 1993;75(10):873-8; Ebert et al., J Biol Chem. 2002 Jul 5;277(27):24609-17). Fluorescence was measured using a fluorometer with an excitation of 360 nm and an emission at 405 nm in the presence or absence of the CathL-inhibitor Z-FF-FMK (10 µM). CathL activity was assessed as the difference between fluorescence with or without CathL-inhibitor.